A critical assessment of the effect of initial fabric on key small-strain design parameters of slurry-deposited silts and sands

C. DOMINGUEZ-QUINTANS[1], J. A. H. CARRARO[2] and L. ZDRAVKOVIC[3]

Abstract

While moist-tamped specimens of silts and sands are most used in engineering practice to characterize tailings, offshore sediments and fluvial/alluvial deposits, design parameters derived from moist-tamping datasets can be significantly different than those obtained from slurry or underwater deposition. This study shows that moist tamped silty and sandy specimens may exhibit phase transformation at stress ratios that are 25 to 50 % lower than those observed for slurry-deposited specimens. Conversely, the small-strain stiffness of the moist tamped specimens tested can be 50% higher than those from slurry deposition. As tailings dams' performance is receiving increased worldwide attention due to recent dam failures in several parts of the world, this study provides new, specific and yet concerning insights about the crucial impact that the selection of moist tamping can have on design parameters. More realistic and rigorous laboratory testing procedures involving tailings remain a key requirement for engineering assessments of tailings behavior. A novel slurry-deposition set-up is presented that allows underwater reconstitution of silts, sands and their mixtures, yielding high-quality uniform specimens. Systematic uniformity checks, which are mandatory to avoid segregation of silty materials, are described. A detailed analysis of typical errors affecting initial void ratio evaluation is also presented to ensure that comparisons between different methods are done with the highest degree of confidence possible.

[1] Corresponding author. Project Engineer. Norwegian Geotechnical Institute (formerly Imperial College London). camelia.dominguez.quintans@ngi.no

[2] Senior Lecturer in Experimental Geotechnical Engineering. Department of Civil and Environmental Engineering, Imperial College London. antonio.carraro@imperial.ac.uk

[3] Professor of Computational Geomechanics. Department of Civil and Environmental Engineering, Imperial College London. l.zdravkovic@imperial.ac.uk

Keywords:

Tailings sands, offshore sediments, specimen reconstitution, slurry deposition, moist tamping.

31 NOTATION

a_j	Aperture of sieve j
D_0	Internal diameter
D_{rc}	Relative density after consolidation
e	Void ratio
E_{dev}	Deviatoric strain ($= 2/\sqrt{3} \cdot (\epsilon_a - \epsilon_r)$)
ϵ_a	Axial strain
ϵ_r	Radial strain
η	Stress ratio ($= q/p'$)
F_{i,a_j}	Percentage of material of slice i passing the sieve with aperture a_j
G_{tan}	Tangent shear stiffness
$H_{s,i}$	Height of slice i
$H_{s,i}/H_t$	Height ratio of the slice i
H_{sp}	Height of the specimen
H_t	Total height available in the compound mixing tube
J	Generalized deviatoric stress ($= q/\sqrt{3}$)
M_s	Mass of dry soil
p'	Mean effective stress ($= (\sigma'_a + 2\sigma'_r)/3$)
q	Deviatoric stress ($= \sigma_a - \sigma_r$)
ρ_s	Density of solids ($= G_s\rho_w$)
ρ_s	Density of slurry ($= M_s/V_t$)
ρ_w	Density of water
S_i	Segregation level of slice i
V_t	Total volume available in the compound mixing tube

32

INTRODUCTION

In engineering practice, laboratory testing of sands usually involves specimen reconstitution as undisturbed sand sampling is only feasible in research and industry projects that can afford expensive site investigation programs. From early (Ladd (1974), Mitchell et al. (1976) and Oda et al. (1978)) to more recent (Vaid et al. (1999), Høeg et al (2000), Ghionna and Porcino (2006), Sze and Yang (2014) and Corrêa and Oliveira Filho (2019)) experimental studies, comparisons among different reconstitution techniques have shown how sand behavior is affected by the applied reconstitution method and by the initial fabric that results from such selection. On the computational side, even the most complex state parameter-based models struggle to rigorously and effectively account for distinct initial fabrics, albeit positive attempts have been made (e.g. Shuttle, 2006; Yang et al., 2008; Loukidis and Salgado, 2009; Li and Dafalias, 2012; Woo and Salgado, 2015; Gao et al., 2019). In geotechnical practice, where complex models may not be frequently used, analyses that support geotechnical design may be deficient if they are based on constitutive model calibration that relies on datasets obtained from specimens whose behavior differs from the behavior of *in-situ* soil.

This paper focuses on the behavior of silts and sands deposited underwater or in slurry environments. These depositional processes are commonly encountered in nature (e.g. fluvial and offshore deposits) as well as in man-made structures such as tailings storage facilities (TSFs) with subaqueous slurry tailings deposition. Experimental evidence comparing the mechanical response of undisturbed (frozen) sand samples to the response of their reconstituted counterparts suggests that water pluviation (WP) is the most suitable technique to reproduce the *in-situ* behavior of poorly-graded clean sands deposited under water (Vaid et al, 1999; Ghionna and Porcino, 2006). However, WP produces non-uniform specimens of well-graded sands or mixtures of sands with fines (Kuerbis and Vaid, 1988). Kuerbis and Vaid (1988) modified WP and created the Slurry Deposition (SD) method to produce high-quality, uniform

specimens of well-graded clean and gap-graded nonplastic silty sands, which was later extended to sands with either plastic or nonplastic fines (Carraro and Prezzi 2007). Recent fundamental research has now demonstrated that SD is the most suitable method to reproduce the initial fabric and mechanical behavior of an undisturbed well-graded clean sand deposited in a fluvial environment (Quinteros and Carraro, 2021; Quinteros, 2022). In this group of rigorous SD methods, in which specimen uniformity is accounted for, a mixing tube is typically used inside which the sample is thoroughly mixed and deposits uniformly within a column of water or slurry. This mixing tube is then inserted into the split mold and the contents of the mixing tube are ultimately transferred to the mold. Rigorous studies that have evaluated specimen uniformity for various slurry deposition methods are summarized in Table 1. Slurry-based methods reported in Table 1 as "limited by tube transfer" refer to the slurry deposition methods that make use of a mixing tube, which requires transferring of the sample from the mixing tube into the split mold. This implies that the achievement of loose states becomes more dependent on operator's skill. Dominguez-Quintans et al. (2019) presented a novel SD apparatus, provisionally developed for small 38-mm-diameter triaxial specimens, where the mold acts as an integral part of the mixing tube. This allows sample deposition to take place directly inside the mold, avoiding tube-to-mold sample transfer and thus unnecessary densification. While real *in-situ* tailings deposition may lead to complex and arbitrary segregation and layering, the use of non-uniform specimens violates the fundamental principle of element testing unless heterogeneity is rigorously controlled (Muir Wood, 2012). So, while crucial, the fundamental understanding of uniform slurry-deposited samples of silty tailings and their states reconstituted using a rigorous slurry deposition method is still lacking.

In practice, most laboratory datasets on tailings are obtained using moist tamping (MT). It is well known that MT leads to highly non-uniform specimens (Frost and Park, 2003), an issue that may be greatly exacerbated if small specimens are used. The significance of initial state

inaccuracies in soil characterization has been highlighted elsewhere (e.g. Li and Coop, 2019) but such errors can be particularly concerning if small specimens are used (Vaid and Sivathayalan 1997). Thus, the issue of carefully assessing soil states for rigorous discussions on the effect of specimen reconstitution is still largely unresolved due to the lack of quality datasets available.

In the present study, the provisional in-mold SD technique, for small specimens originally described in Dominguez-Quintans et al. (2019), was further developed and validated, for the first time, for larger 70-mm-diameter specimens for both silts and sands. New findings from this state-of-the-art technique are then compared to those obtained for specimens reconstituted using a well-described MT technique (Frost and Park, 2003). Systematic reexamination of this issue through the use of a novel in-mould, larger 70-mm-diameter SD specimens, has finally allowed for any empirical differences observed in the mechanical response to be solely attributed to the reconstitution method used. This has never been attempted before using a rigorous in-mould SD method, particularly in the case of slurry silts and/or silty sands.

This paper first introduces a new slurry-based method to determine the maximum void ratio and then describes a novel rigorous in-mold SD reconstitution method for 70-mm-diameter triaxial specimens of both silts and sands. Subsequently, experimental uncertainties related to void ratio assessments are critically evaluated. Finally, results of undrained triaxial tests using the novel in-mold SD method and a conventional MT technique are examined and their implications to geotechnical analysis and design of TSFs are discussed in light of expected biases in design parameters due to the reconstitution method selected for a given analysis.

MATERIALS TESTED AND MAXIMUM VOID RATIO OF SLURRY

A uniform clean quartz sand from the UK, namely Ham River sand (HRS) as described by Takahashi and Jardine (2007), and a soil mixture containing 5 % (by mass) of HRS and 95 %

of nonplastic quartz sandy silt HPF5 were tested. This tailings-like analogue blend, named tailings sandy silt (TSS), has a gradation that is similar to the gradation of many tailing materials, such as those used for testing programs that followed the failures of Fundão (Morgenstern et al. 2016), Cadia (Jefferies et al., 2019) or Feijão (Robertson et al., 2019) dams. Index properties and particle size distributions (PSDs) of the samples tested are shown in Table 2 and Fig. 1, respectively.

The method used to determine the maximum void ratio of a soil significantly affects the e_{max} values, similar to the effect of different reconstitution methods on the initial fabric of specimens subjected to mechanical testing. It is therefore instructive for a site investigation program to attempt to relate these methods as well as possible to the *in-situ* deposition of the materials being characterized. Higher void ratios with other methods that create a different fabric are possible (e.g. under unsaturated conditions), but would not represent a feasible state under conditions of underwater deposition. This is important to the extent that e_{max} affects the determination of relative density, which can have implications if the interpretation of in-situ states (e.g. CPT-based) are correlated to relative density. As mentioned above, real in-situ deposition of tailings materials, for example, will be affected by complex segregation, but the method presented herein attempts to simulate this type of underwater deposition only to achieve uniform elements. The e_{max} procedures used in this study are improved versions of the original slurry e_{max} method proposed by Carraro and Prezzi (2007). For clean HRS, the device used, suitable to determine a uniform sample of e_{max} for uniform and gap-graded soils of up to 15 % fines content, is shown in Fig. 2(left). This device comprises an acrylic mold and an acrylic collar attached to the mold using adhesive tape. The collar has a drainage hole in its lower end that is temporarily sealed with adhesive tape. Fresh de-aired water is used to fill the device up to the collar mid-height. A funnel is placed at the collar top and the sample is poured into the funnel held at all times above the water level (a tentative dry mass of sand required to loosely

fill the mold leads to the highest underwater void ratio possible). Next, the collar is topped up with fresh de-aired water and the top cap is installed with its valve open. Then, the valve is closed, the device is turned up and down and around its axis several times. The device is refilled with de-aired water and the process repeated until the sample is completely de-aired. When the mixed soil-water suspension looks homogeneous, the device is turned upside down and back upright one more time and finally placed gently on a stable benchtop. The sample is allowed to settle vertically inside the device. Once the sample fills the mold, the top valve is opened and the tape sealing the drainage hole removed allowing the extra water/slurry to drain out slowly. The tape attaching the collar and mold is removed, and the collar is gently taken away. The soil in the mold is then carefully levelled off and the oven-dried mass of soil filling the mold is determined. Full schematic representation on the complete procedure is shown in Fig. 2 (centre). For the given device diameter, the collar length was optimized to ensure that the maximum void ratio of uniform/gap-graded soil slurries can be obtained using this procedure ($e_{max,SD}$).

Underwater/slurry pluviation of well-graded sands and silts in low viscosity water/slurry environments, like the one created by the method described above, induces particle segregation (Kuerbis and Vaid, 1988). Consequently, measurements using this method are not representative of uniform specimens of soil which should usually be considered in element testing. To avoid this, e_{max-SD} determination for TSS was conducted using the 38-mm-diameter density gradient mold described in Dominguez-Quintans et al. (2019). In this alternative procedure, a short collar is used (Fig. 2-right). The amount of TSS required for this procedure is derived from the uniformity analysis described later, which ensures uniform TSS specimens are obtained. In this procedure, water is replaced by 2.1% gelatin solution (by mass), as recommended by Emery et al. (1973). Gelatin use details and how to successfully minimize its impact on results are described elsewhere (e.g. Emery et al. 1973; Kuerbis and Vaid, 1988;

157 Carraro and Prezzi, 2007; Tastan and Carraro, 2013). The resulting slurry TSS sample is then
158 thoroughly mixed by turning the device upside down and back up for about 15 minutes. Finally,
159 the device is gently placed on a stable benchtop and the sample is allowed to settle and solidify
160 overnight at room temperature (~20 +/- 1 ^{o}C). The device was subsequently kept in a
161 refrigerator at 5 ^{o}C for 3 hours before slicing the two lowermost layers (3 and 4) used to
162 determine $e_{max\text{-}SD}$.

163 SPECIMEN RECONSTITUTION

164 ***In-mold slurry deposition***

165 Uniformity analysis

166 A key advantage of SD over WP is that SD allows reconstitution of uniform specimens of well-
167 graded sands and sands with fines (Kuerbis and Vaid, 1988; Carraro and Prezzi, 2007). This
168 group of SD methods (Kuerbis and Vaid, 1988; Carraro and Prezzi, 2007; Tastan and Carraro,
169 2013; Dominguez-Quintans et al., 2019) rely on the use of a larger amount of material than
170 what will be needed to fill the reconstitution mold. Therefore, uniformity analyses must precede
171 testing to ensure that the amount of soil, water content, collar height and mixing time used are
172 properly defined to produce uniform slurries. This analysis was conducted with a 38-mm-
173 diameter 4-layer density gradient mold for the clean uniform HRS tested in this study
174 (Dominguez-Quintans et al., 2019). Due to its low Cu (Table 2), high uniformity levels can be
175 achieved for HRS even at relatively low slurry densities. However, segregation is expected to
176 happen during uncontrolled pluviation through water/slurry of well-graded sands or sands with
177 fines and/or silty materials such as the TSS analogue, as well as for most tailings from real
178 slurry tailings dams. SD only eliminates segregation if an appropriate slurry density (ρ_{slurry})
179 is used during reconstitution. To illustrate this, four uniformity analyses were performed using
180 slurry densities ranging from 890 up to 1300 kg/m^3. ρ_{slurry} is defined as the ratio of dry mass

of soil (M_s) to the total volume (V_t) of the mixing device (Fig. 3a). The density gradient mold described in Dominguez-Quintans et al. (2019) was used here with an additional slice (#0) above the specimen top (#1), to enlarge sample column to ensure specimen uniformity.

Specimens used in these uniformity analyses were prepared with de-aired water and allowed to partially desaturate at room temperature (20 ± 0.5 °C) for 24 hours by leaving the specimen top uncovered and bottom drainage line (Fig. 2-right) open to the atmosphere. Relatively small particle sizes in the samples enabled slicing the layers with a thin wire saw without interlayer collapse due to the small capillary suction that develops within the unsaturated specimens. Each slice's void ratio was determined for all uniformity specimens tested based on the internal volume and oven-dried mass of each slice (Fig. 4). The lower the slurry density the lower the uniformity exhibited, with most non-uniform specimens displaying decreasing density with increasing slice elevation – even for the top layers that are not part of the specimen but that are also included for completeness (Fig.4a-b). Some of these top slices have void ratios that are even higher than $e_{max\text{-}SD}$ because the observed non-uniformity is also related to systematic segregation (i.e., the higher the slice, the finer the material (Fig.5), as in a hydrometer test) and to the particle sizes in these top slices not representative of the TSS gradation (Fig.5). The specimen with the most uniform density (Fig. 4d) does no longer show a trend of segregation with height and shows a maximum variation in void ratio across the height of 0.05. This is consistent with other SD studies with uniformity analyses (e.g. Bradshaw and Baxter, 2006; Wang et al., 2011), and the results of this study are well placed within the silt category (see Table 1).

The PSDs of all slices tested were determined by wet sieving (ASTM D6913/D6913M–17) down to a sieve opening of 36 μm and compared to the PSD of the original TSS (Fig. 5). To assess the segregation induced by different slurry densities, the difference between the PSD curve for each slice (i) and the PSD of the original TSS sample was determined. Each

206 "integration interval" corresponds to the difference of the logarithm to the base 10 of two
207 consecutive sieve apertures (i.e., a_{j+1} and a_j). The segregation S_i for slice i is expressed as:

$$S_i \approx \sum_j 0.5 \cdot \left(\left(F_{i,a_{j+1}} - F_{i,a_j}\right) + \left(F_{TSS,a_{j+1}} - F_{TSS,a_j}\right)\right) \cdot \left(\log\left(\frac{a_{j+1}}{a_j}\right)\right) \quad (1)$$

208 where a_j is the sieve aperture, F_{i,a_j} is the percentage of material of slice i passing sieve aperture
209 a_j, and F_{TSS,a_j} is the percentage of the TSS passing sieve aperture a_j.

210 Segregation values obtained using this method are plotted in Fig. 3b as a function of
211 dimensionless parameters: height ratio ($H_{s,i}/H_t$), as shown in Fig. 3a, and slurry density ratio
212 (ρ_{slurry}/ρ_s), where ρ_s is the density of the solids. As shown in Fig. 3b and Fig. 5, segregation
213 reduces as the slurry density increases, with 1300 kg/m^3 yielding a uniform specimen that
214 matches the target gradation of TSS. While the slurry density was the key parameter governing
215 sample preparation quantities for the 70-mm-diameter TSS specimens tested, the normalized
216 parameters in Fig.3b may provide insight into required quantities for other materials. As a result
217 of this analysis, in the case of silts, for a typical 2:1 (height:diameter) triaxial specimen to be
218 completely uniform (from bottom to top), the slurry mixing volume must be equal to twice the
219 final specimen volume for a slurry density equal to half of the density of the solid phase of the
220 sample being tested.

221 Modified triaxial base pedestal

222 Pilot and preliminary tools for the in-mold SD method for small 38-mm-diameter specimens
223 are described in Dominguez-Quintans et al. (2019). For that set-up, the base pedestal with
224 external drainage lines was easily detachable from the triaxial cell base. In the present study,
225 this in-mold concept was developed further for a new 70-mm triaxial cell with a larger (and
226 heavier) base pedestal and internal drainage lines. The original pedestal was split into a
227 shortened pedestal (SP) and a new transition piece (TP) (Fig. 6a), acting temporarily as a base

pedestal during reconstitution. The two side pins in the TP work in two ways: (1) when fully inserted (Fig. 6b), a rubber sleeve seals the vertical lines. At the same time, bottom lateral drainage during densification is possible through one pin (Fig. 6b close up). Alternatively, (2) when mixing is completed and the TP is placed on top of SP, the pins are moved outwards and locked by splitters, clearing the vertical lines (Fig. 6a). When the test is running, O-rings seal the horizontal holes (Fig. 6a close up).

Procedure

This new SD reconstitution method is carried out using the mixing tube set-up shown in Fig. 7 and follows the steps below:

1) The TP is detached from the SP with pins fully inserted (Fig. 7). The split mold is set up over a latex membrane sealed at the bottom against the TP by two O-rings. The membrane is rolled over the mold top and vacuum is applied to the space between membrane and mold.
2) The collector is placed over the membrane-covered mold top and the collar is installed on top of the collector and split mold. The collar-to-mold clamp then holds the whole device together. The collar-to-split mold interface is sealed with an O-ring housed within the collar base.
3) The mixing tube is half-filled with fresh deaired water and the predefined amount of dry soil (derived from the uniformity analysis) is slowly poured in to minimize air entrapment.
4) The mixing tube is topped up with deaired water and a sealing cap is placed on top. This cap has a drainage hole that allows extra water to come out freely. The hole is then temporarily sealed with adhesive tape.

5) The whole device is thoroughly mixed for as long as it is needed for its contents to form a homogeneous slurry. Special care must be taken at this step for the TSS sample (or any well-graded soil sample) which typically requires 15 to 20 minutes of mixing time, whereas less than a minute is sufficient for the clean HRS.
6) The whole device is carefully placed back onto the SP so that the TP securely sits on the locating step designed to join these two parts (Fig. 6a). Pins are moved outwards, and the splitters are installed to clear the vertical drainage holes (Fig. 6a). The slurry mixture is allowed to settle until clear water is seen in the upper part of the collar (Fig. 7 photo). This step may take as long as 90 minutes for the TSS tested in this study.
7) The cap tape is removed and the cap is carefully taken away. Extra water in the collar top is removed with a suction bottle. The collar-to-mold clamp is released, and the collar is gently withdrawn. Extra soil above the mold top is levelled with the mold top using a thin knife in two sideway motions from centre, after which the collector is removed and the exposed membrane cleaned. Special care must be taken during levelling off of the specimen top to limit possible densification of the upper part of the specimen, as noted by Thomson and Wong (2008).
8) Specimen reconstitution is now completed (typically after 1 h for HRS or 2-3 h for TSS) and the filter paper, porous stone and top cap are installed. The membrane is rolled over the top cap and sealed by a pair of O-rings while the cap is temporarily held by a holding frame to minimize specimen top disturbance. All specific details about the experimental procedure can be found in Dominguez-Quintans (2022).

Moist tamping with undercompaction

The MT specimens were tamped in 7 layers according to Frost and Park (2003). The HRS specimens were prepared with 5 % water content and 1 % undercompaction ratio. For the TSS material, the two loosest specimens used 5 % water content and 3 % undercompaction, whereas

276 the water content of denser specimens was increased to 10 % to facilitate tamping. These
277 parameters were selected following a series of pilot tests employing a range of
278 undercompaction ratios and water contents. For all HRS and two loosest TSS specimens, a 40-
279 mm-diameter tamper was used with a reference stopper to control the height of each layer. For
280 the denser TSS specimens, manual tamping was not sufficient to achieve required densities and
281 a load frame was used with the 40-mm-diameter tamper.

282 TRIAXIAL TESTING

283 Triaxial testing was performed on 70-mm-diameter 140-mm-height specimens using a
284 computer-controlled triaxial stress path cell. Detailed calibration errors of all transducers can
285 be found in Dominguez-Quintans (2022). Internal on-specimen instrumentation consisted of
286 two axial and one radial linear variable displacement transformer (LVDT) transducers.

287 All specimens underwent flushing, back-pressure saturation until a minimum B-value of 0.97,
288 and isotropic consolidation before undrained shearing. Right-cylinder correction based on
289 local-strain instrumentation data was suitable to calculate specimen deformation up to at least
290 phase transformation. Due to end restraints, specimen deformation after phase transformation
291 was mainly associated with barreling. At this stage, Lade's (2016) mid-height area correction
292 was used.

293 ***Critical assessment of specimen states***

294 Errors due to equipment calibration and initial specimen dimensions

295 The initial void ratio of each specimen was calculated from the dry mass measured at the end
296 of the test and the height and diameter measurements obtained after reconstitution and under
297 the 20-kPa vacuum. Subsequent void ratio changes due to all disturbance stages applied before
298 consolidation were tracked through the high-resolution local instrumentation. Considering the
299 maximum calibration errors, the minimum resolvable volumetric strain with internal

300 instrumentation (0.07 %) leads to a maximum void ratio error of 0.002, which corresponds to
301 a 0.8 to 0.9 % error in relative densities for HRS.

302 Additionally, the variability in the estimation of relative density due to initial specimen
303 dimension variations was estimated to be around 3 % (0.007 error in void ratio). This derived
304 from an analysis carried out for one HRS specimen whose height and diameter were measured
305 10 and 20 times, respectively. The best estimate of relative density was then compared to
306 relative density estimations from 5 randomized observations taken from the measurement pool
307 using the typical number of height and diameter measurements (5 and 6, respectively) used in
308 the experimental program. Thus, pairs in Table 3 can be considered comparable.

309 Errors due to saturation

310 For all stages before consolidation, changes in specimen height were typically interpreted based
311 on the average strain resulting from the two local, axial LVDTs, whereas diameter changes
312 were resolved from the radial strain belt readings. During consolidation, given that specimens
313 are fully saturated and to account for possible non-uniformities, particularly in the case of MT
314 specimens, the radial strain was resolved based on the volumetric strain measured by the back
315 pressure volume gauge and the internal average strain data from the two local, axial LVDTs.
316 A summary of all specimen void ratios after reconstitution, saturation and consolidation are
317 displayed in Table 3.

318 As it has been pointed out by Sladen and Handford (1987) and extensively highlighted by
319 others (e.g., Jefferies and Been, 2006; Been et al., 1991; Verdugo and Ishihara, 1996) void ratio
320 changes experienced by MT specimens during saturation can be as large as those experienced
321 during consolidation, particularly when fines are present and loose states are of concern (see
322 MT8 data). The void ratio of the loosest MT8 specimen is the maximum achievable using
323 manual tamping. Such unrealistically high void ratios are only possible due to the suction-

related capillary bonds that develop in these unsaturated specimens (Vaid et al., 1999). Under saturated conditions, these states are not feasible, thus a noticeable reduction in void ratio ensues (Table 3). If a thorough assessment of void ratio changes during saturation is not carried out, testing results associated with very loose MT specimens that are initially unsaturated may be inaccurately reported (Fig. 8a). Another major consequence of this error would be its direct effect on the CSL estimation, as schematically illustrated in Fig. 8b. It should be noted that the CSL shown here is just hypothetical and this is not intended to replace the real identification of the CSL of the TSS. Table 4 summarizes various studies on the comparisons among reconstitution methods, which show that this saturation-induced error may have not been always considered. The accuracy of the void ratio assessment methods used is also not clearly quantified in many studies.

ANALYSIS OF RESULTS AND DISCUSSION

Maximum void ratios from slurry deposition

The maximum void ratio achieved with the new SD method proposed in this study (e_{max_SD}) is assumed to be more representative of the loosest state associated with deposition under water for a non-segregated sample than those obtained with dry samples as prescribed in ASTM D4254-16 and other standard testing methods. It is important to note that *in-situ* states may be however affected by segregation, layering, etc. Thus, caution should be taken by practitioners when interpreting and using this loosest state by appreciating that such procedure is only applicable to samples of uniform (i.e. poorly-graded) soils. For HRS, the coefficient of variation (COV) obtained using the slurry method is 1.0 % from 9 trials, indicating a repeatability level comparable to the 0.7 % resulting from 10 trials with the ASTM dry determination (Table 2). For clean uniform sands such as HRS, the void ratio values achieved with the proposed method exceed those obtained with the dry ASTM determinations. This

suggests that the lower depositional energy imparted during particle deposition under water for clean uniform sands leads to lower minimum densities than those obtained through dry placement methods.

On the other hand, the slurry-based maximum void ratio COV of the tailings sandy silt was 3.8 % for 3 determinations using a gelatin solution of 2.1 % concentration. Likewise, a total of 11 determinations using a wider range of gelatin concentrations (from 1.4 to 2.3 %) produced the same void ratio average and a COV of 3.6 %. Dry ASTM D4254-16 determination for this material produced a higher maximum void ratio with a COV of 1.4 % from a total of 6 trials. This inverse trend in the slurry and dry maximum void ratios of the TSS compared to that observed for clean HRS suggests that the possible states achievable from dry deposition of finer materials cannot exist under saturated conditions. Note that the water content used in the slurry for TSS has an impact on the void ratio value obtained. The water content used was based on the target slurry density, selected to ensure specimen's uniformity with TSS gradation.

Isotropic compression

Following initial specimen reconstitution and saturation to $p' = 20$ kPa, isotropic compression was the first controlled mechanical disturbance to take place. Therefore, it crucially helps understand fabric differences among reconstitution methods. Vaid et al. (1999) showed much higher 1-D compressibility of their MT specimens compared to the water pluviated or air pluviated ones under initially very loose states. Isotropic triaxial data have the added advantage that it can offer insights into the strains developed in different directions. For both soils tested, Fig. 9 indicates that an anisotropic response is observed with higher horizontal compressibility. Additionally, the radial strains developed by the MT specimens are consistently higher than those from the SD ones (possibly due to the higher vertical stresses required during tamping) with this difference decreasing with decreasing particle size.

372 ***Undrained triaxial response of Ham River Sand (HRS)***

373 Fig. 10 shows the undrained triaxial compression response of HRS specimens reconstituted by
374 MT and SD. Loose specimens with post-consolidation relative densities around 42 % (test pairs
375 1, 3 and 5 in Table 3) were subjected to three levels of mean effective stress at the end of
376 isotropic consolidation (p'_c = 100, 400 and 600 kPa). Additional results for specimens with
377 post-consolidation relative density around 60 % (test pairs 2 and 4 in Table 3) are also shown
378 for levels of p'_c equal to 100 and 400 kPa. All stress paths are plotted in Fig. 10a, stress-strain
379 responses are plotted in Fig. 10b and compression plane responses in Fig. 10c. Fig. 10c also
380 provides the symbols identifying key states: start of test, undrained instability (UI), phase
381 transformation (PT), peak stress ratio and end of test. For all tests with comparable states, MT
382 specimens consistently show a more dilative response than their SD counterparts at earlier
383 stages of the tests, such as UI and PT. The behavioral divergencies at PT states were evaluated
384 plotting the normalized differences in mean effective stresses (Fig. 11a); stress ratios (Fig. 11b)
385 and axial strains (Fig. 11c) against p'_c. Fig. 11a suggests that differences in mean effective
386 stress at PT induced by the reconstitution method increase markedly with decreasing density
387 and moderately with increasing p'_c. Furthermore, MT specimens phase transform at lower
388 stress ratios and smaller strains, a divergency that decreases markedly with increasing p'_c and
389 moderately with increasing density (Fig. 11b and 11c). The initial more contractive tendencies
390 developed by the SD specimens compared to the MT specimens are eventually counteracted
391 by a distinctively higher post-PT dilative trend, leading to similar stresses when critical states
392 are approached (Fig. 10b and 10c).

393 At first sight, this may appear to be in contradiction with another systematic study that has
394 shown greater strain softening during undrained behavior for MT specimens compared to their
395 pluviated counterparts (i.e. Vaid et al., 1999). However, Vaid et al. (1999) studied specimens

under very loose states. Trends derived from studies where comparisons of MT specimens with a broader range of densities (e.g., Tsukamoto et al (1998) with water sedimentation on gravelly samples, Papadimitriou et al. (2005) and Wichtmann and Triantafyllidis (2015) with air pluviation) qualitatively agree with the findings shown herein, where the MT specimens show an initially stiffer behavior compared to their pluviated counterparts. Nevertheless, MT is often not standardized or carefully described in terms of the number of layers, undercompaction ratio, water content, tamper dimensions, tamping stresses required for specimen reconstitution and procedures used. For example, out of the 13 studies reported in Table 5 in which MT was used, only 2 thoroughly reported all the above-mentioned details. Furthermore, regardless of whether these are reported completely or partially, they usually differ from laboratory to laboratory even if classified under the same MT umbrella. This makes comparison with other publications involving MT specimens rather difficult.

Undrained triaxial response of Tailings Sandy Silt (TSS)

The undrained triaxial compression responses of TSS specimens are plotted in Fig. 12, with similar plots as in Fig. 10 for HRS. For this material, both 100 (pair 6 in Table 3) and 400 kPa (pair 7) consolidation levels were tested with SD and MT methods, with SD7-R being a repeatability test for SD7, together with two looser MT specimens consolidated to 400 kPa (MT8 and repeatability test MT8-R). The latter two specimens illustrate classic examples of flow liquefaction: stresses are markedly reduced following UI until a very low (but non-zero) value is sustained (~ 15-20 kPa) – although these values must be taken with caution due to the difficulties in accurately quantifying axial stress at the end of these tests. All other MT specimens tested in this study, whose post-consolidation void ratios are comparable to their SD counterparts, phase transform and reach peak stress ratio at earlier axial strains (Fig. 12b). As shown by the HRS data, MT specimens of TSS are more dilative and phase transform at lower stress ratios than their SD counterparts (inserts in Fig. 12a). This contradicts the findings from

Correa and Oliveira Filho (2019) on tailing silts, but, once again their tested relative densities ranged from loose to very loose (up to 35 %). Fig. 11 reveals that disparities among methods for the finer TSS follow similar trends with respect to the consolidation mean effective stress to those observed for clean HRS. However, the magnitude of the divergency is consistently higher than that of HRS at comparable relative densities (around 60 %). This might suggest that the influence of the reconstitution method on the undrained shearing response is greater for silts than it is for sands. This may be explained by considering the higher compressibility exhibited by the TSS compared to HRS, which might imply a larger effect of the tamping on the mechanical behaviour.

It is important to note that for MT specimens (considering the water content and other relevant parameters used in the MT reconstitution procedure described above) to achieve similar void ratios to those of their SD specimen counterparts, the tamping vertical stresses were as high as 1000 up to 4000 kPa, according to the load cell records used during tamping. Recent studies on quarzitic materials revealed that particle crushing is not expected below 10 MPa (Zheng and Tannant, 2016). However, the effect of these high tamping efforts must be taken into consideration as they lead to over-consolidation of MT specimens. This impacts initial stiffness and leads to very early shear band development, as discussed in Frost and Park (2003), a fact that was apparent for MT6 and MT7, especially for post-peak stages, as illustrated in Fig. 11.

Stiffness degradation behavior

Fig. 13 plots the degradation of tangent shear stiffness (G_{tan}) with increasing axial strain. G_{tan} was deduced from the tangent slopes of the generalized deviatoric stress ($J = q/\sqrt{3}$) with increasing deviatoric strain ($E_{dev} = 2/\sqrt{3}(\epsilon_a - \epsilon_r)$). As shown for the HRS specimens in Fig. 13a, MT stiffnesses are systematically larger than the stiffness of SD specimens. MT specimens tend to phase transform (square) when the stiffness is not close to 0, as opposed to the SD

specimens. Whenever UI (triangle) was observed, its stiffness demarks the state up to which almost full stiffness degradation has already taken place, with little additional stiffness degradation observed afterwards. Otherwise, this lower bound limit of stiffness degradation appears to be set by the stiffness at PT or between PT and peak stress ratio (diamond) states.

Similar conclusions to the ones outlined above can be drawn for the TSS specimens. However, the MT results consistently show substantially higher shear stiffness throughout the tests compared to the SD results, as shown in Fig. 13b, but now with the peak stress ratio (diamond) demarking the lower bound stiffness level after which minimal additional degradation takes place.

Potential implications to the engineering design of TSFs

While some of the SD specimens of silt and sand tested in this study may not show UI for the specific states tested, they systematically exhibit around 50 % lower stiffness than MT counterparts, particularly at strains smaller than 0.01 % (Fig. 13). Additionally, the stress ratio at phase transformation of SD specimens is around 25 % to 50 % higher than that of MT specimens (Fig. 11b), with SD strains at this stage about 100 % larger than those of MT specimens (Fig. 11c). If this is integrated into a numerical analysis, larger strains and lower strengths will be mobilized early on if SD data is used instead of MT. Overall, this suggests that if the MT method with the details and procedures presented here would be used in design practice, this approach may be unconservative.

In practice, some version of MT is often adopted in assessments of tailings dam failures (e.g., Morgenstern et al., 2016, Robertson et al., 2019, Jefferies et al., 2019). Justification for this usually relies on the relative simplicity of MT and the good control of initial overall specimen density, especially to achieve loose states. The typical inability of either the WP or SD techniques to achieve very loose initial states that can be of relevance to real TSF (Shuttle and

469 Cunning, 2007) has been a fair criticism of these methods. But high *in-situ* field void ratios
470 inferred from CPT analysis may also be due to segregation (Fig 4a), if layering is not correctly
471 captured, for example, due to an insufficiently small cone penetrometer tip. The e_{max_SD} (from
472 uniform elements) may be a more relevant limit, despite the artificial values that can be
473 achieved with unsaturated, non-uniform MT specimens, typically related to saturation-induced
474 collapse. This is not to say that the method does not have its own limitations as it, for example,
475 does not capture layering or segregation, so this is an important aspect to keep in mind from
476 the practitioners' point of view. The method developed in this investigation attempts to push
477 these limits further – with its own further limitations owing to laboratory-related restrictions –
478 while fulfilling the criteria outlined by Kuerbis and Vaid (1988) regarding reconstitution
479 method suitability: (a) void ratio and particle size uniformity and (b) representativeness of *in-*
480 *situ* soil conditions. Both key criteria, unfortunately, are not satisfied by MT methods: even if
481 well controlled, MT layering is unavoidable (as described in Frost and Park (2003)) and MT
482 representativeness for tailings materials has never been proven (as opposed to pluviated
483 methods, as shown in Vaid et al. (1999)). Finally, the present study also shows that SD
484 responses are not necessarily always more dilative than MT. When rigorous methods are
485 adopted, as outlined in the present study, MT response can be more dilative than SD (Fig
486 13a,b). But this finding does require a great degree of control of the methods used, in order for
487 all variables of relevance to be kept the same, except for the method-imparted initial fabric.

488 The present study analyzed the triaxial response of the silt and sand materials tested. This has
489 been performed in a high-quality manner and has demonstrated a strong effect of the
490 reconstitution method on the specimens' strength and stiffness. However, understanding the
491 behavior of a real TSF is more complex than the result of any laboratory element test, which
492 cannot be simply extrapolated to predict the actual mechanism happening in the field. This can
493 only be assessed through computational analyses of boundary value problems that are based

494 on sound constitutive models that, in turn, are calibrated using a representative dataset of
495 geomaterial behavior from rigorous laboratory and *in-situ* testing programs.

496 CONCLUSIONS

497 An experimental program was conducted to identify key differences in the mechanical response
498 of slurry deposited and moist tamped specimens. A reconstitution method that simulates
499 underwater/slurry deposition for sands and silty materials, as it is commonly found in slurry
500 tailings deposits and deposits of alluvial, fluvial and offshore sediments, is described and
501 critically assessed in this study. The results of this investigation emphasize the following:

502 A) A novel in-mold slurry deposition method is presented that is able to produce looser
503 uniform specimens than previous slurry deposition methods. Loose states are relevant
504 for many applications, one important example is the case of in-situ slurry tailings
505 deposits. The achievement of looser states is now possible because the new proposed
506 method does not rely on thick consolidating slurries typically used for reconstitution of
507 silts (not to be confused with slurry deposition), which inherently compromise the
508 attainment of looser states. The new method also minimizes potential densification by
509 eliminating sample transfer from the mixing tube to the split mold. This new slurry
510 deposition method describes all the necessary and crucial developments required to test
511 larger 70-mm diameter specimens of slurry-deposited silts and sands, like the invention
512 of a novel transition piece and the effective unification of the extension collar and split
513 mold into a single unit.
514 B) A process of systematic identification of errors associated with the measurements used
515 in this study is outlined. This allowed post-consolidation states achieved for pairs of
516 comparable triaxial specimens in this study to be virtually identical, allowing
517 systematic comparisons between initial fabrics to be made.

C) A novel detailed analysis of the process required for the determination of a suitable choice of slurry density in the mixing device is presented for the first time, which is a crucial requirement to reconstitute uniform specimens from slurry/underwater deposits. This new analysis focuses on the uniformity of void ratio and particle size distribution across the specimen height. The method presented herein does not violate one of the most crucial aspects of element testing: specimen uniformity. For silts and the specimen-to-mixing tube volume ratio used in this study (1:2), the slurry density that should be used to achieve a uniform specimen is half the density of the particles tested. Potential segregation and layering may occur in underwater deposition *in-situ* and this topic deserves further rigorous study.

D) A new procedure to assess the loosest states achievable in slurry/underwater environments is proposed for non-segregated specimens, leading to values that are higher (for the sand) or lower (for the silt) than those obtained with standard testing methods on dry samples. For loose states, void ratios reported in the geotechnical literature or commercial practice may be much higher than they might actually be if derived from methods that do not properly account for saturation-induced volume changes and slurry/underwater deposition. Nevertheless, real, *in-situ* deposition in TSFs may be prone to segregation and further rigorous research on this topic is needed.

E) For the systematic moist-tamping reconstitution technique used in this study, the stress level induced by tamping may play a substantial role on specimen response at early stages of shearing; this effect should be quantified as it may lead to otherwise unnoticed over-consolidation effects. Furthermore, the number of variables that may play a role on moist-tamping reconstitution methods is much higher than what is typically reported or discussed in the literature (i.e., number of layers, undercompaction ratio, water content, tamping dimensions, tamping stresses and other procedures used). Each one of

these variables (including the over-consolidation, which effectively relates to fabric changes) will ultimately define the fabric of the final MT specimens. Such discussions lack in the moist-tamping literature.

F) Selection of a reconstitution method that is representative of uniform slurry/underwater deposition is highlighted to support numerical analyses of real TSFs. This is because the initial fabric due to specimen reconstitution has a real impact on stiffness. For the silt and sand tested, an initially less dilative response was observed for the slurry-deposited specimens compared to their moist-tamped counterparts, with differences of about 50% in terms of initial stiffness and about 25 to 50% for stress ratio at phase transformation. Stiffness at undrained instability reduces to negligible amounts. These results demonstrate that, when the initial states are virtually identical, specimens prepared by moist-tamping are not always more liquefiable than slurry-deposited specimens, as it may have been shown in the past.

DATA AVAILABILITY STATEMENT

All data that support the findings of this study are available from the corresponding author upon request.

ACKNOWLEDGEMENTS

This PhD research and the lead author were supported by a Skempton Scholarship from the Department of Civil and Environmental Engineering at Imperial College London. The authors would like to thank Mr. S. Karapanagiotidis for the technical support in manufacturing the equipment.

565 REFERENCES

566 Ahmadi Naghadeh, R., & Toker, N. K. (2019). Exponential equation for predicting shear
567 strength envelope of unsaturated soils. *International Journal of Geomechanics*, 19(7),
568 04019061.

569 Baldi, G., Hight, D. W., & Thomas, G. E. (1988). State-of-the-art paper: a reevaluation of
570 conventional triaxial test methods. *Advanced triaxial testing of soil and rock*. ASTM
571 International.

572 Been, K., Jefferies, M. G., & Hachey, J. (1991). The critical state of sands. *Géotechnique*,
573 41(3), 365-381.

574 Bradshaw, A. S., & Baxter, C. D. P. (2007). Sample preparation of silts for liquefaction testing.
575 *Geotechnical Testing Journal*, 30(4), 324-332.

576 Carraro, J. A. H., & Prezzi, M. (2007). A new slurry-based method of preparation of specimens
577 of sand containing fines. *Geotechnical Testing Journal*, 31(1), 1-11.

578 Chang, N., Heymann, G., & Clayton, C. (2011). The effect of fabric on the behaviour of gold
579 tailings. *Géotechnique*, 61(3), 187-197.

580 Corrêa, M. M., & Oliveira Filho, W. L. (2019). Impact of methods used to reconstitute tailings
581 specimens on the liquefaction potential assessment of tailings dams. *REM-International*
582 *Engineering Journal*, 72(3), 507-513.

583 Dominguez-Quintans, C. (2022). *Static and cyclic characterisation of sandy and silty soils*
584 *deposited underwater*. PhD thesis. Imperial College London.

585 Dominguez-Quintans, C., Quinteros, S., Carraro, J. A. H., Zdravkovic, L., Jardine, R.J. (2019).
586 Quality assessment of a new in-mould slurry deposition method for triaxial specimen
587 reconstitution of clean and silty sands. *E3S Web of Conferences*, 92, 02010.

588 Donahue, J., Bray, J., & Riemer, M. (2007). Liquefaction testing of fine-grained soil prepared
589 using slurry deposition. *Proceedings of the 4th International Earthquake Geotechnical*
590 *Engineering, Thessaloniki, Greece*, Paper, 1226.

591 Frost, J. D., & Park, J. Y. (2003). A critical assessment of the moist tamping technique.
592 *Geotechnical Testing Journal*, 26(1), 57-70.

593 Gao, Z., Zhao, J., Li, X. S., & Dafalias, Y. F. (2014). A critical state sand plasticity model
594 accounting for fabric evolution. *International journal for numerical and analytical methods in*
595 *geomechanics*, 38(4), 370-390.

596 Ghionna, V. N., & Porcino, D. (2006). Liquefaction resistance of undisturbed and reconstituted
597 samples of a natural coarse sand from undrained cyclic triaxial tests. *Journal of Geotechnical*
598 *and Geoenvironmental Engineering*, 132(2), 194-202.

599 Head, K. H. (1998). Manual of soil laboratory testing. Volume 3: effective stress tests (No. Ed.
600 2). *John Wiley & Sons*.

601 Høeg, K., Dyvik, R., & Sandbækken, G. (2000). Strength of undisturbed versus reconstituted
602 silt and silty sand specimens. *Journal of Geotechnical and Geoenvironmental Engineering*,
603 126(7), 606-617.

604 Jefferies, M., & Been, K. (2006). *Soil liquefaction: a critical state approach*. CRC press.

605 Jefferies, M, Morgenstern, N. R., Van Zyl, D., & Wates, J. (2019). *Report on NTSF*
606 *Embankment Failure*. Cadia Valley Operations for Ashurst Australia.

607 Knudsen, S., Lunne, T., Quinteros, S., Vestgården, T., Krog, L., Bøgelund-Pedersen, R. (2019).
608 Effect of reconstitution techniques on the triaxial stress-strength behaviour of a very dense
609 sand.

Krage, C. P., Price, A. B., Lukas, W. G., DeJong, J. T., DeGroot, D. J., & Boulanger, R. W. (2020). Slurry Deposition Method of Low-Plasticity Intermediate Soils for Laboratory Element Testing. *Geotechnical Testing Journal*, 43(5).

Kuerbis, R., & Vaid, Y. P. (1988). Sand sample preparation-the slurry deposition method. *Soils and Foundations*, 28(4), 107-118.

Ladd, R. S. (1974). Specimen preparation and liquefaction of sands. *Journal of Geotechnical and Geoenvironmental Engineering*, 100 (Proc. Paper 10857 Proceeding).

Li, W., & Coop, M. R. (2019). Mechanical behaviour of Panzhihua iron tailings. *Canadian Geotechnical Journal*, 56(3), 420-435.

Li, X. S., & Dafalias, Y. F. (2012). Anisotropic critical state theory: role of fabric. *Journal of Engineering Mechanics*, 138(3), 263-275.

Loukidis, D., & Salgado, R. (2009). Modeling sand response using two-surface plasticity. *Computers and Geotechnics*, 36(1-2), 166-186.

Mitchell, J. K., Chatoian, J. M., & Carpenter, G. C. (1976). The influence of fabric on the liquefaction behaviour of sand. *Report to US Army Engineer WES*.

Morgenstern, N. R., Vick, S. G., Viotti, C. B., & Watts, B. D. (2016). *Fundão tailings dam review panel report on the immediate causes of the failure of the Fundão dam*. Cleary Gottlieb Steen & Hamilton LLP, New York.

Muir Wood, D. (2012). Heterogeneity and soil element testing. *Géotechnique Letters*, 2(3), 101-106.

Oda, M., Koishikawa, I. & Higuchi, T. (1978). Experimental Study of Anisotropic Shear Strength of Sand by Plane Strain Test. *Soils and Foundations*, 18(1), 25–38.

632 Papadimitriou, A. G., Dafalias, Y. F., & Yoshimine, M. (2005). Plasticity modeling of the
633 effect of sample preparation method on sand response. *Soils and foundations*, 45(2), 109-123.

634 Quinteros, V. S (2022). *On the initial fabric and triaxial behaviour of an undisturbed and*
635 *reconstituted fluvial sand*. PhD Thesis, Imperial College London.

636 Quinteros, V. S., & Carraro, J. A. H. (2021). The initial fabric of undisturbed and reconstituted
637 fluvial sand. *Géotechnique*, 1-40.

638 Reid, D., & Fanni, R. (2020). A comparison of intact and reconstituted samples of a silt tailings.
639 *Géotechnique*, 1-13.

640 Robertson, P.K, De Melo, L, Williams, D. J., & Wilson, G. W. (2019). *Report of the Expert*
641 *Panel on the Technical Causes of the Failure of Feijão Dam I*.

642 Shuttle, D. A. (2006). Can the effect of sand fabric on plastic hardening be determined using a
643 self-bored pressuremeter? *Canadian Geotechnical Journal*, 43(7), 659-673.

644 Shuttle, D. A., & Cunning, J. (2007). Liquefaction potential of silts from CPTu. *Canadian*
645 *Geotechnical Journal*, 44(1), 1-19.

646 Sladen, J. A., & Handford, G. (1987). A potential systematic error in laboratory testing of very
647 loose sands. *Canadian Geotechnical Journal*, 24(3), 462-466.

648 Sze, H. Y., & Yang, J. (2014). Failure modes of sand in undrained cyclic loading: impact of
649 sample preparation. *Journal of Geotechnical and Geoenvironmental Engineering*, 140(1), 152-
650 169.

651 Takahashi, A., & Jardine, R. J. (2007). Assessment of standard research sand for laboratory
652 testing. *Quarterly Journal of Engineering Geology and Hydrogeology*, 40(1), 93-103.

653 Tastan, E. O., & Carraro, J. A. H. (2013). A new slurry-based method of preparation of hollow
654 cylinder specimens of clean and silty sands. *Geotechnical Testing Journal*, 36(6), 811-822.

655 Thomson, P. R., & Wong, R. C. K. (2008). Specimen nonuniformities in water-pluviated and
656 moist-tamped sands under undrained triaxial compression and extension. *Canadian*
657 *Geotechnical Journal*, 45(7), 939-956.

658 Tsukamoto, Y., Ishihara, K., & Nonaka, T. (1998). Undrained deformation and strength
659 characteristics of soils from reclaimed deposits in Kobe. *Soils and Foundations*, 38(Special),
660 47-55.

661 Vaid, Y. P., & Sivathayalan, S. (1997). Errors in estimates of void ratio of laboratory sand
662 specimens. *Canadian Geotechnical Journal*, 33(6), 1017-1020.

663 Vaid, Y. P., Sivathayalan, S., & Stedman, D. (1999). Influence of specimen-reconstituting
664 method on the undrained response of sand. *Geotechnical Testing Journal*, 22(3), 187-195.

665 Verdugo, R., & Ishihara, K. (1996). The steady state of sandy soils. *Soils and Foundations*,
666 36(2), 81-91.

667 Wang, S., Luna, R., & Stephenson, R. W. (2011). A slurry consolidation approach to
668 reconstitute low-plasticity silt specimens for laboratory triaxial testing. *Geotechnical Testing*
669 *Journal*, 34(4), 288-296.

670 Wichtmann, T., & Triantafyllidis, T. (2015). An experimental database for the development,
671 calibration and verification of constitutive models for sand with focus to cyclic loading: part
672 I—tests with monotonic loading and stress cycles. *Acta Geotechnica*, 11(4), 739-761.

673 Woo, S. I., & Salgado, R. (2015). Bounding surface modeling of sand with consideration of
674 fabric and its evolution during monotonic shearing. *International Journal of Solids and*
675 *Structures*, 63, 277-288.

Wood, F. M., Yamamuro, J. A., & Lade, P. V. (2008). Effect of depositional method on the undrained response of silty sand. *Canadian Geotechnical Journal*, 45(11), 1525-1537.

Xu, L., & Coop, M. R. (2017). The mechanics of a saturated silty loess with a transitional mode. *Géotechnique*, 67(7), 581-596.

Yang, Z. X., Li, X. S., & Yang, J. (2008). Quantifying and modelling fabric anisotropy of granular soils. *Géotechnique*, 58(4), 237-248.

Zheng, W., & Tannant, D. (2016). Frac sand crushing characteristics and morphology changes under high compressive stress and implications for sand pack permeability. *Canadian Geotechnical Journal*, 53(9), 1412-1423.

Zlatovic, S., & Ishihara, K. (1997). Normalized behaviour of very loose non-plastic soils: effects of fabric. *Soils and Foundations*, 37(4), 47-56.

Fig 1

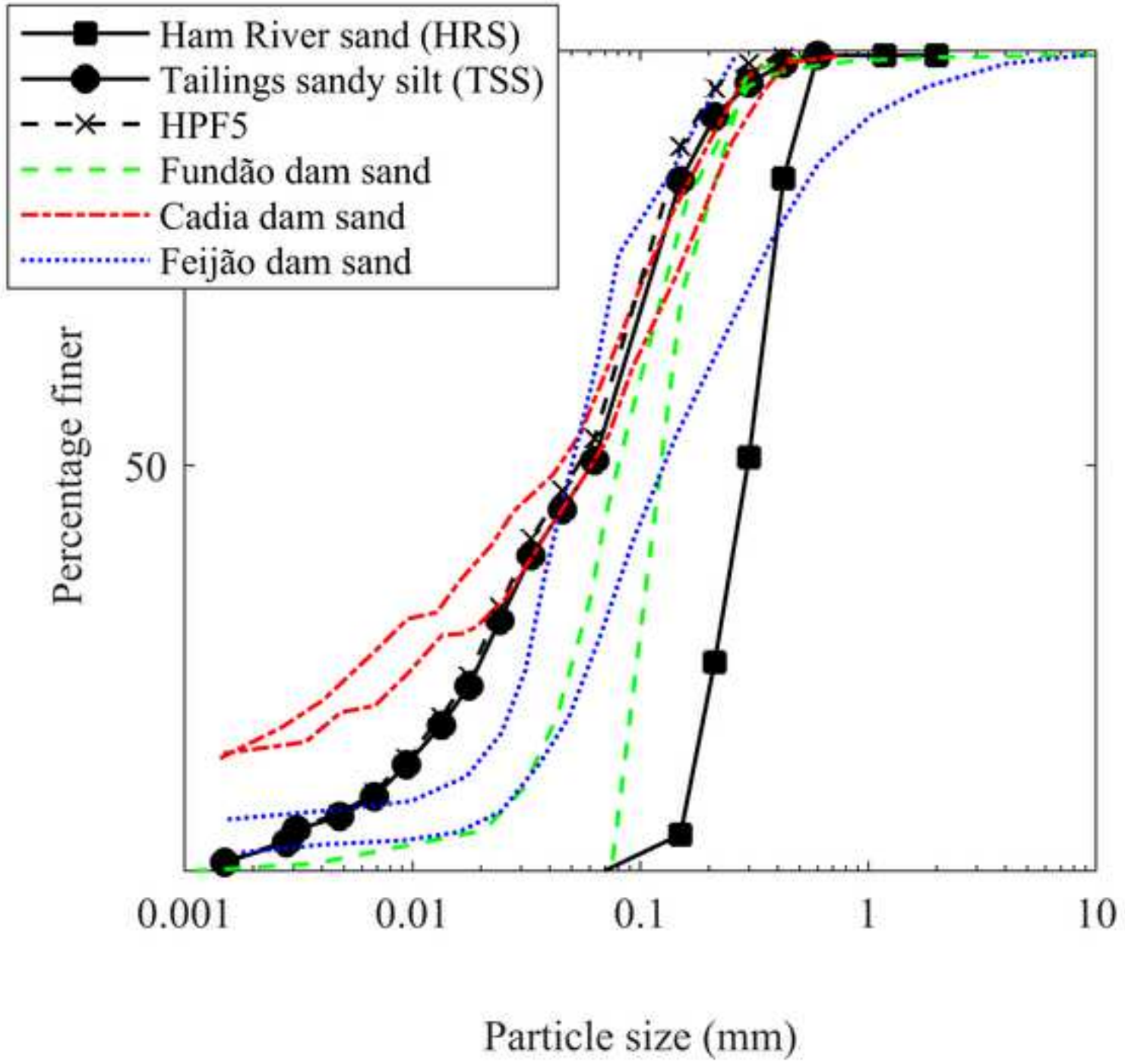

Fig 2

Click here to access/download;Figure;Fig 2.tif

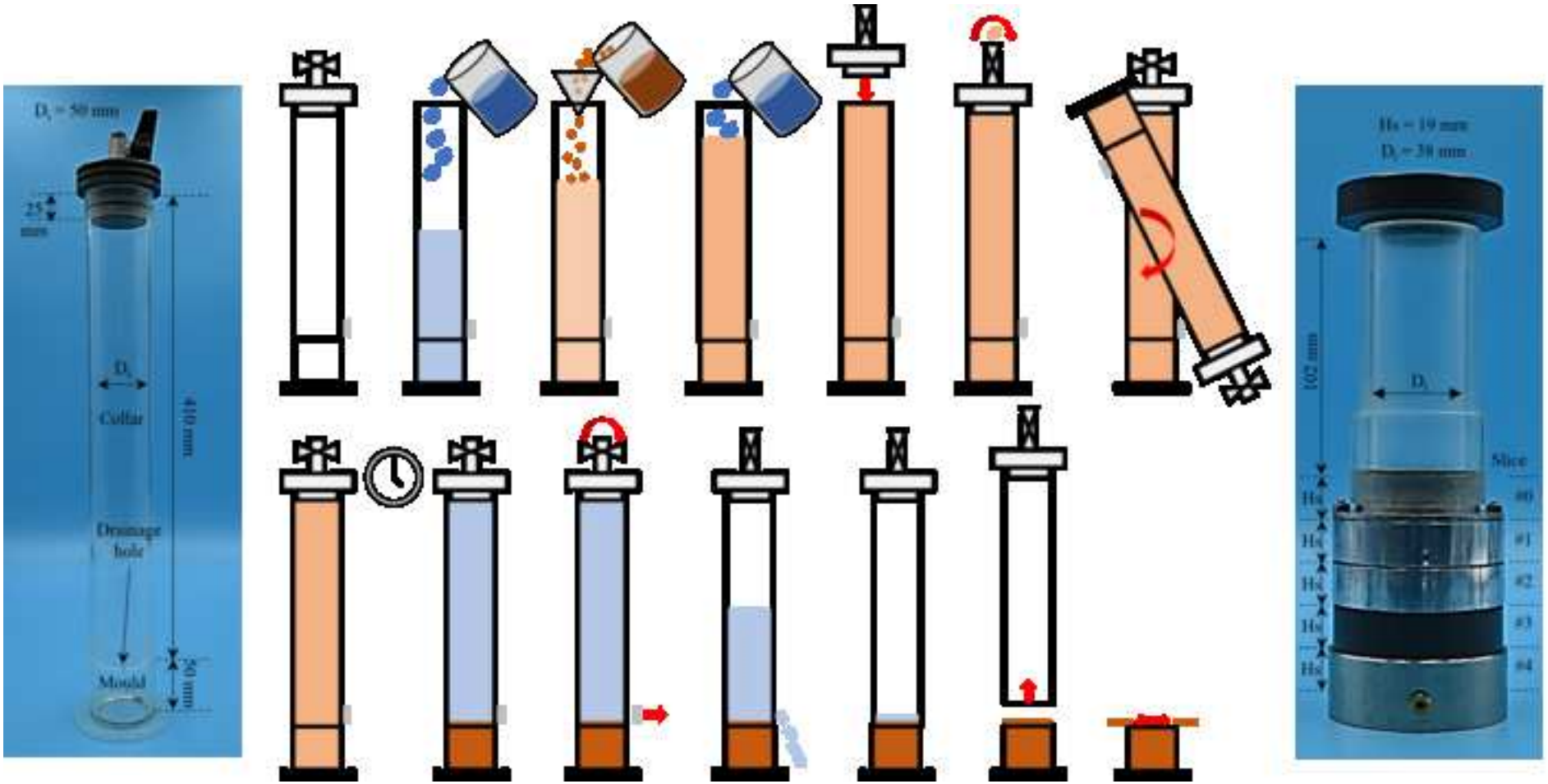

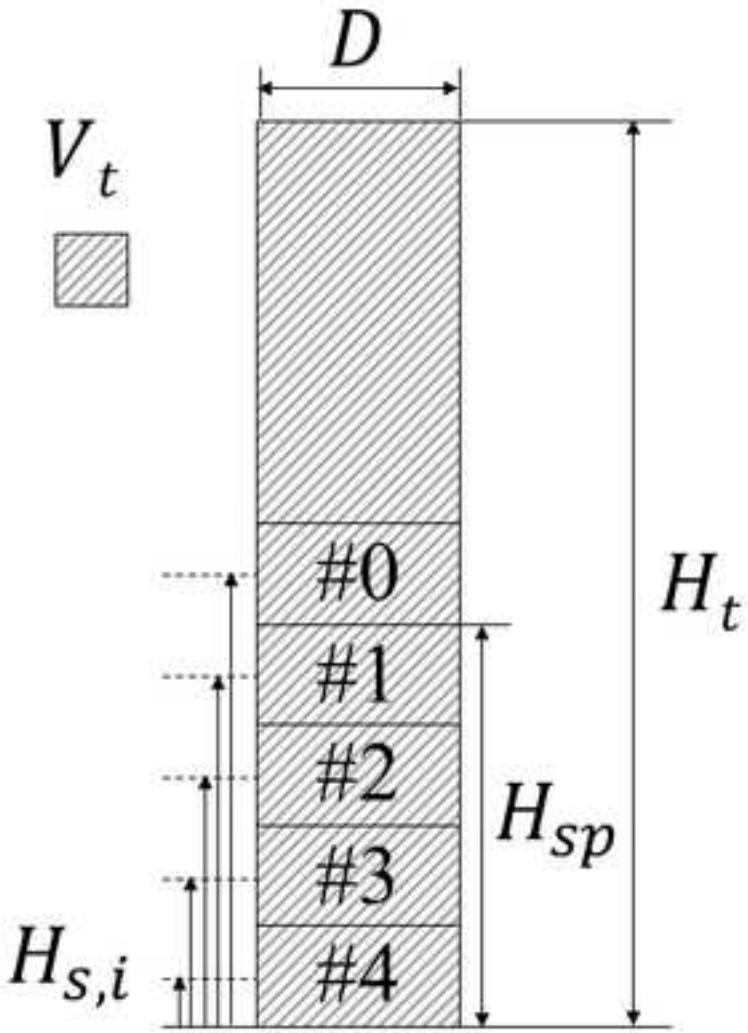

$$V_t = \pi \cdot \frac{D^2}{4} \cdot H_t$$

Fig 3b

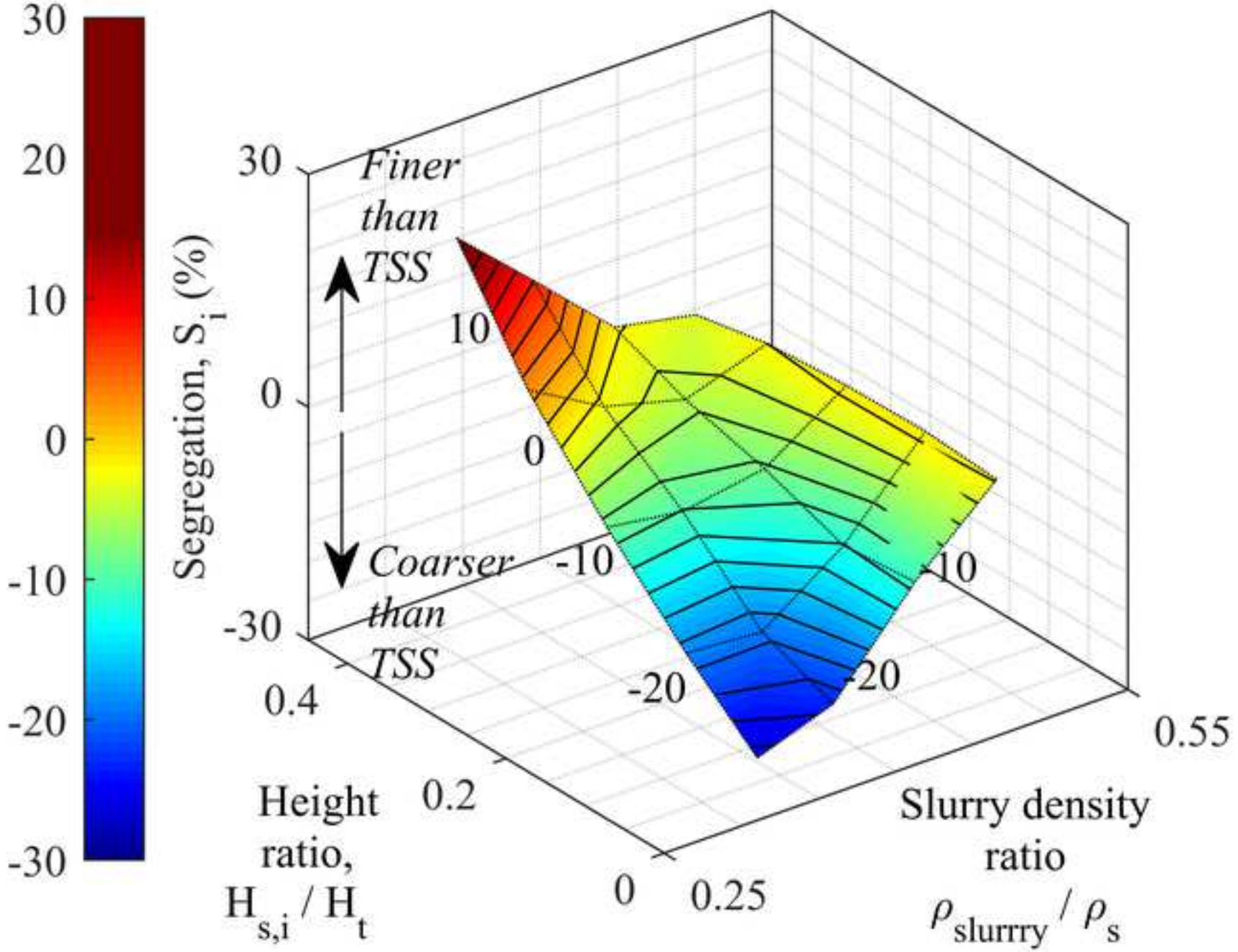

Fig 4

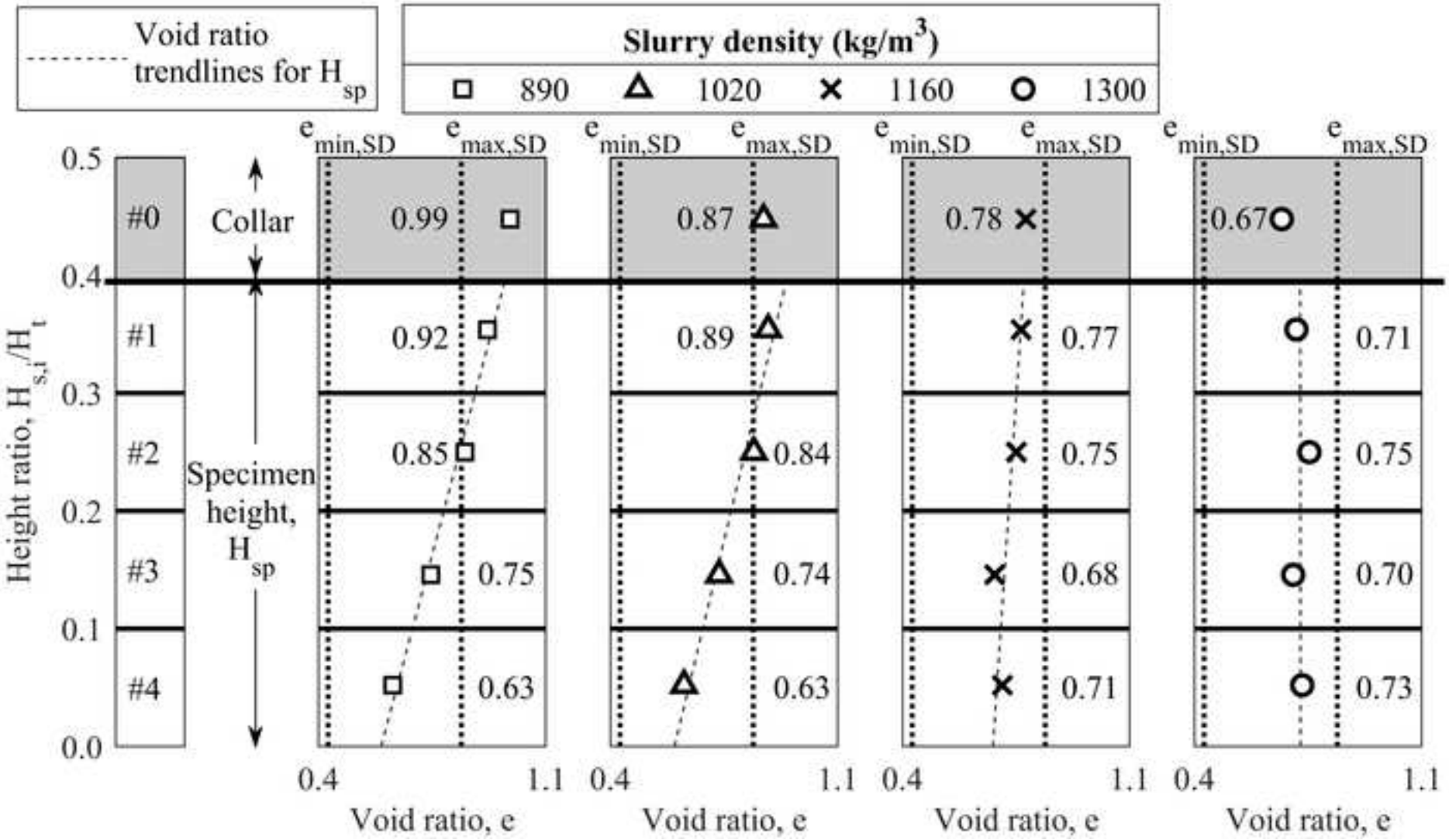

Fig 5

Click here to access/download;Figure;Fig 5.tif

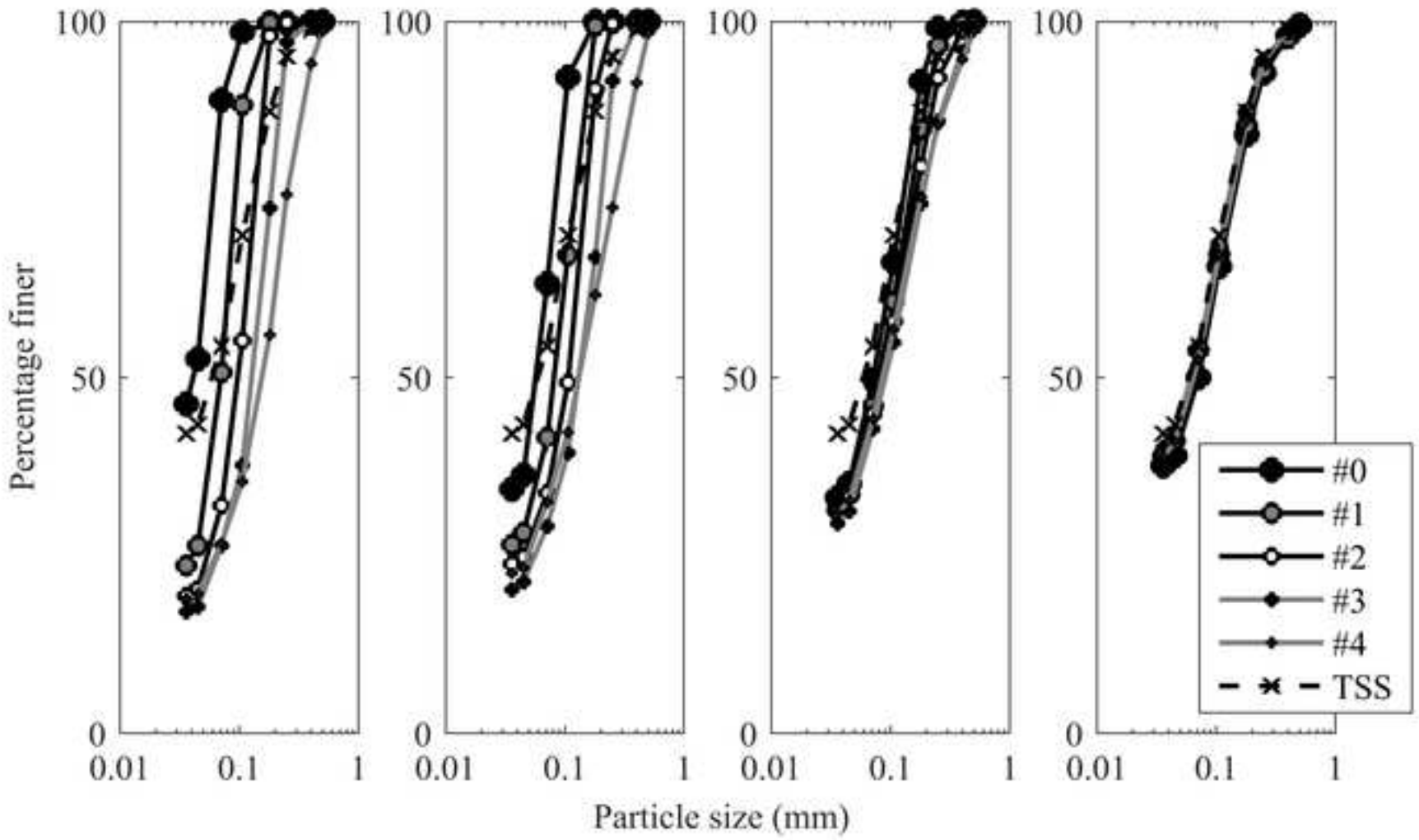

Fig 6a

Click here to access/download;Figure;Fig 6a.tiff

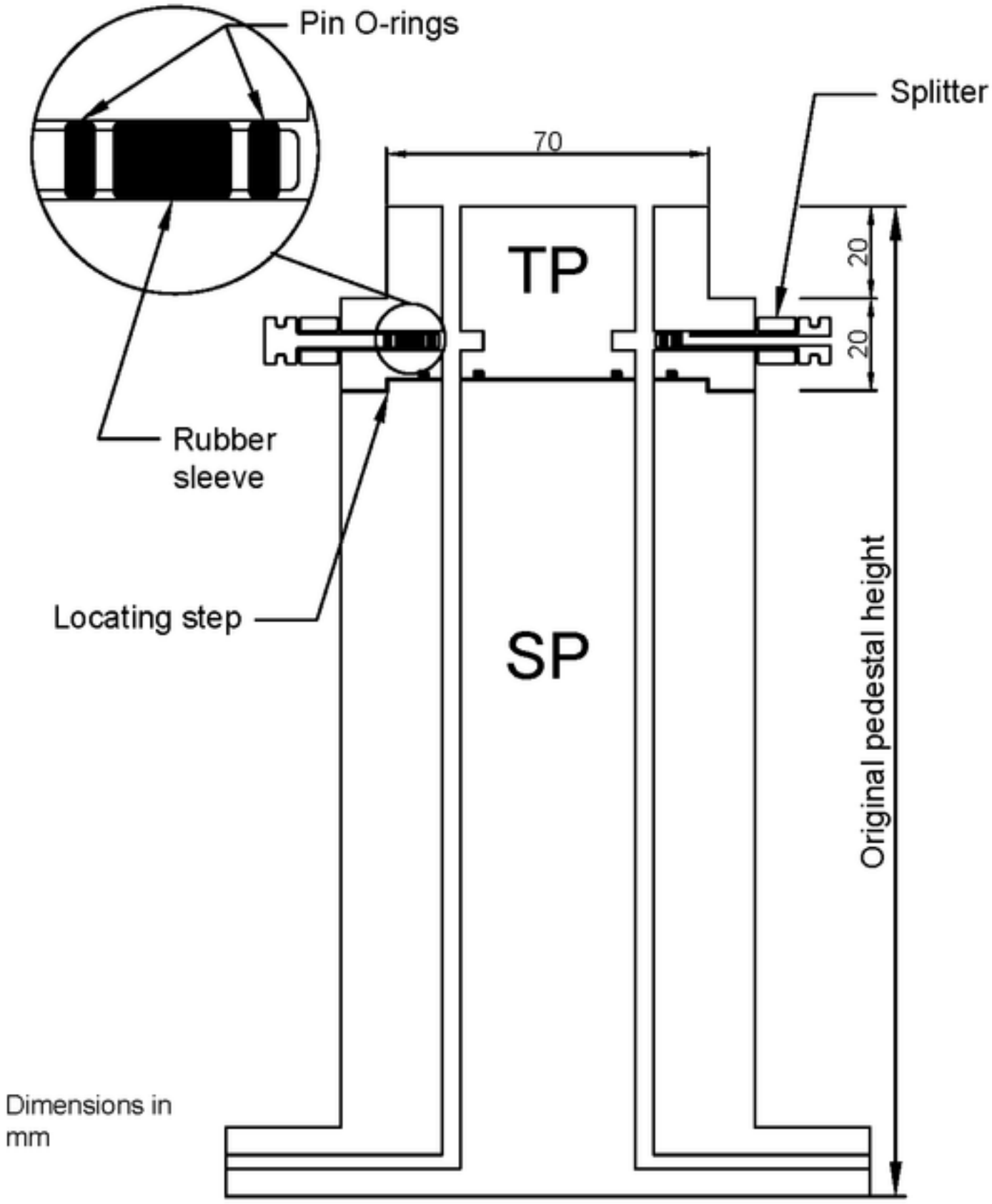

Fig 6b

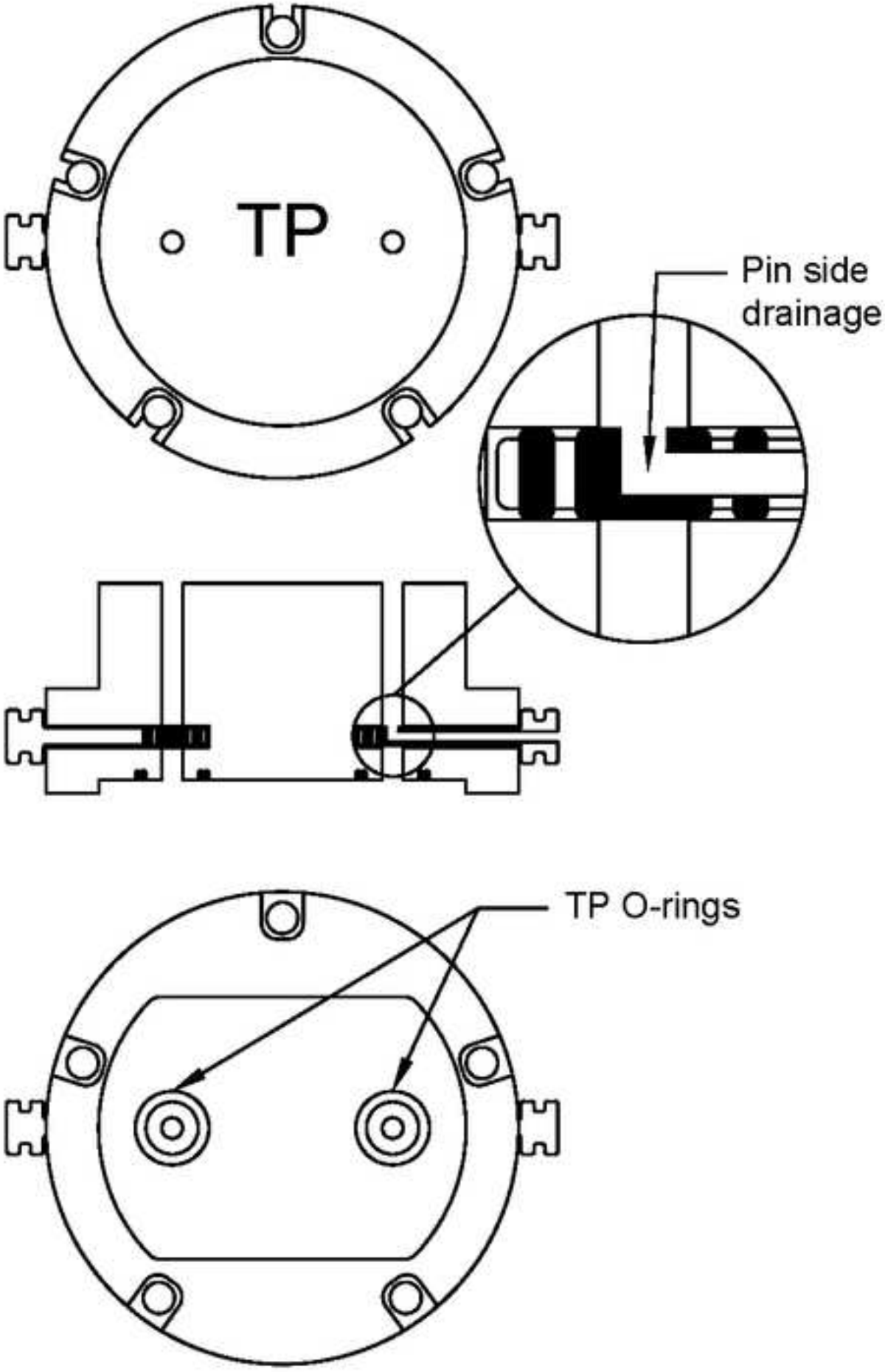

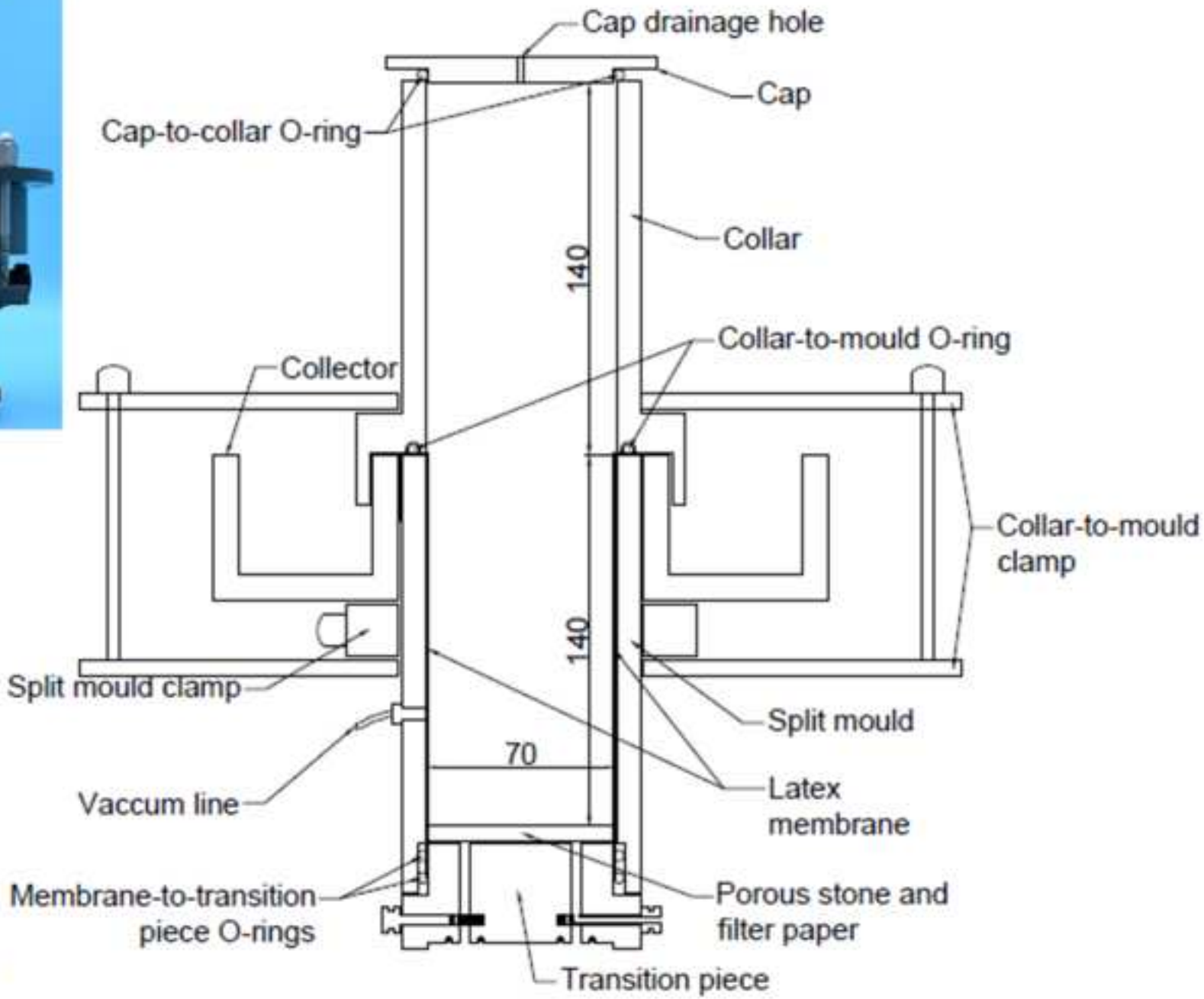

Dimensions in mm

Fig 8a

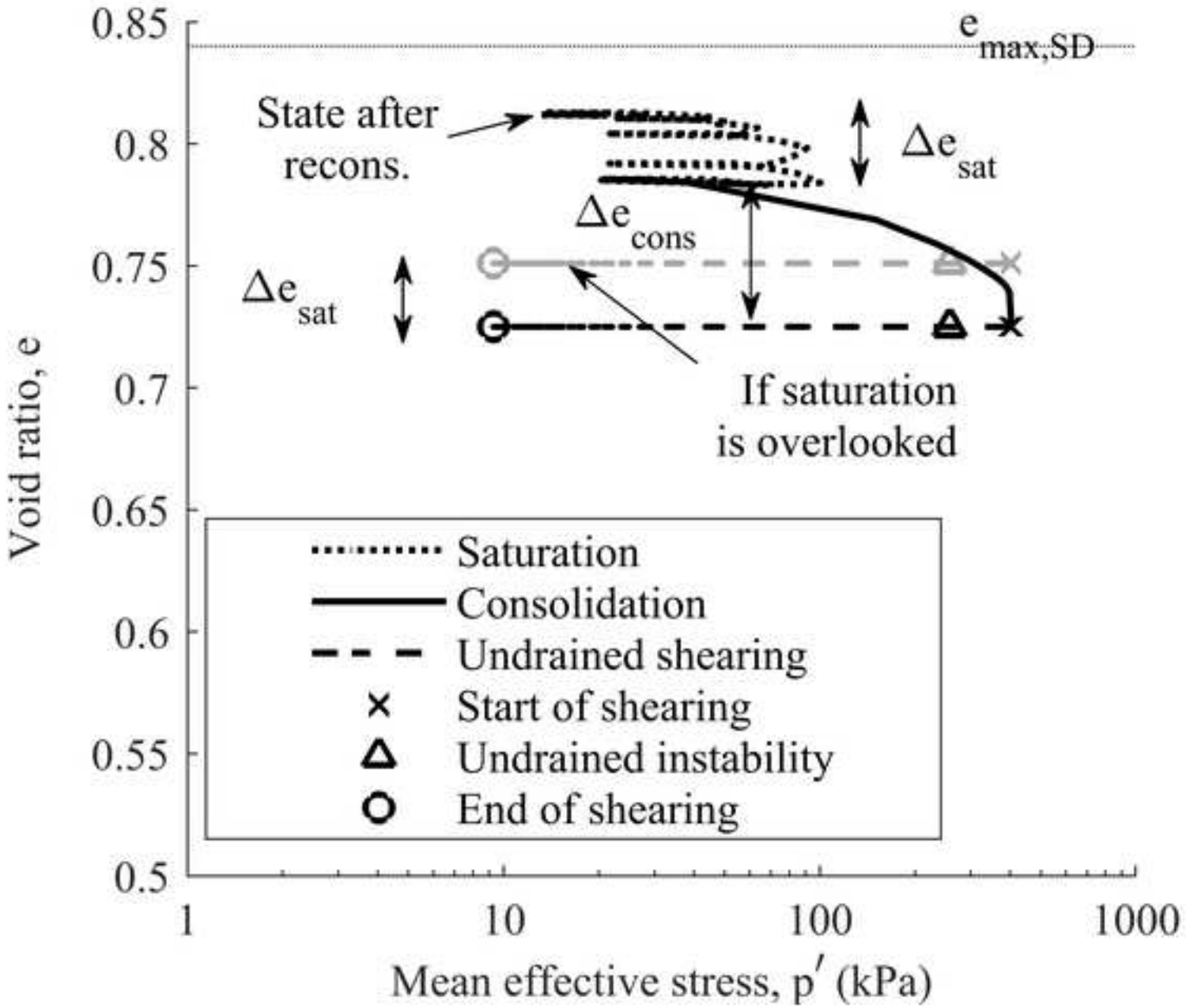

Fig 8b

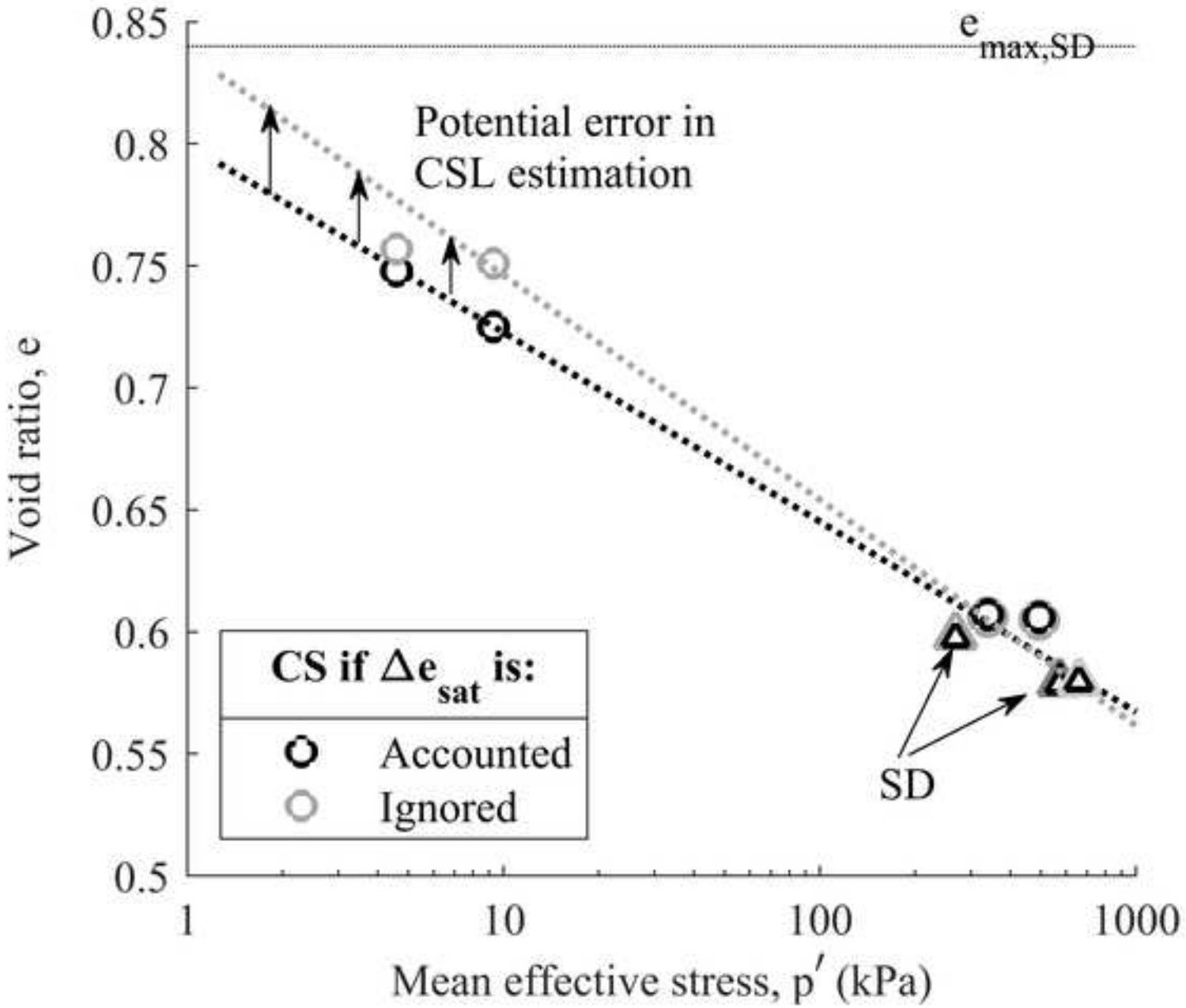

Fig 9

Click here to access/download;Figure;Fig 9.tif

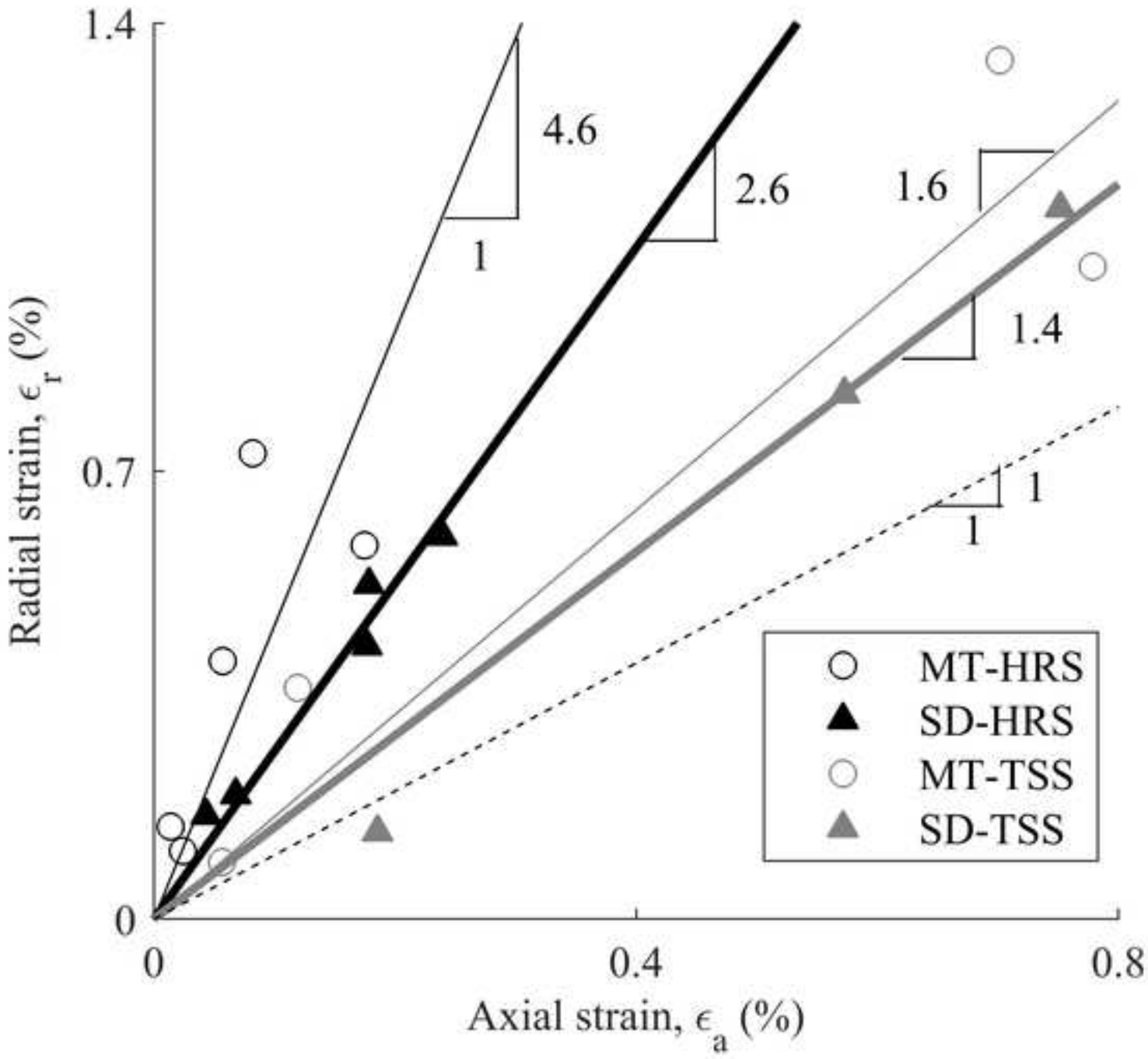

Fig 10a

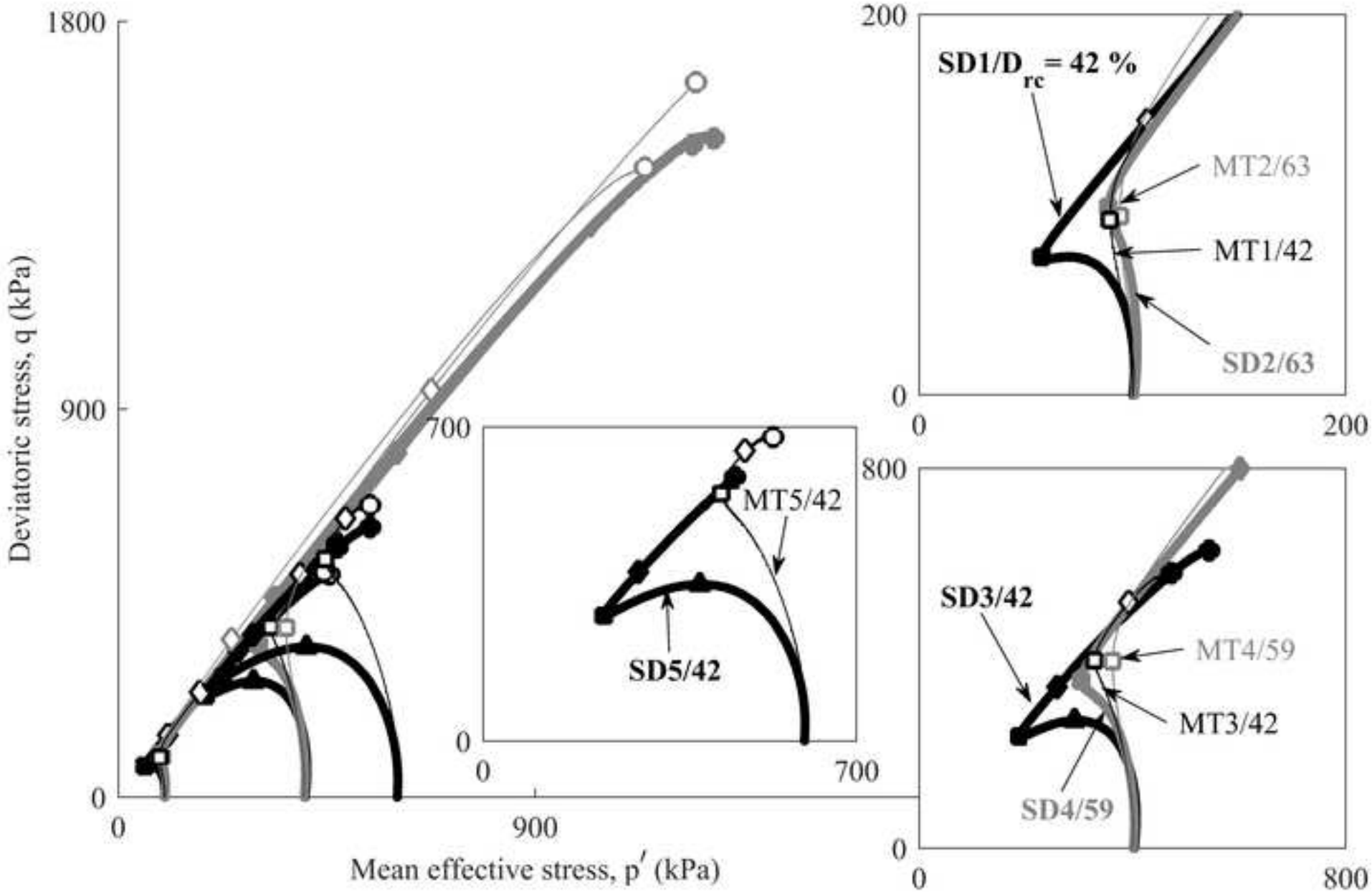

Fig 10b

Click here to access/download;Figure;Fig 10b.tif

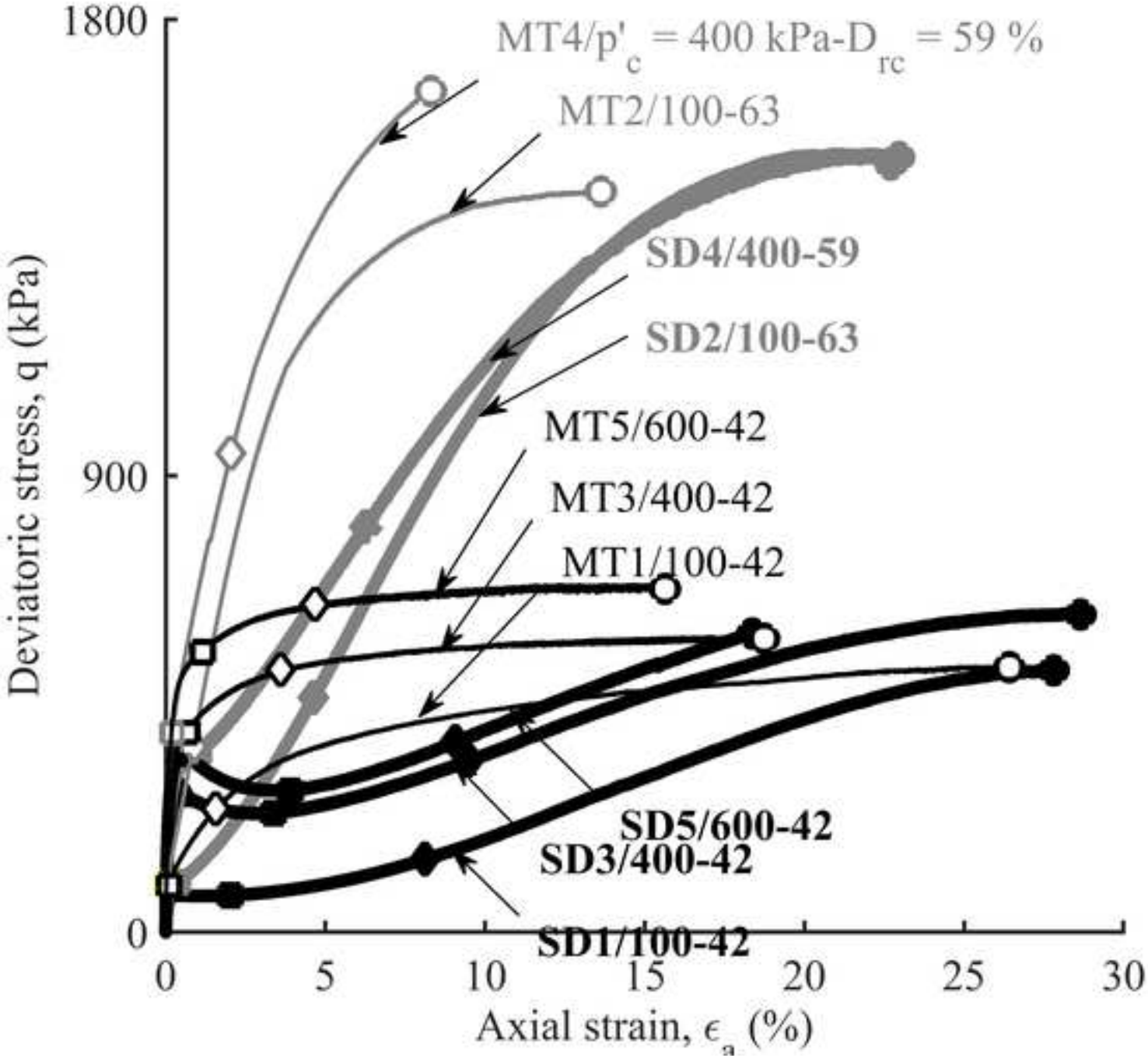

Fig 10c

Click here to access/download;Figure;Fig 10c.tif

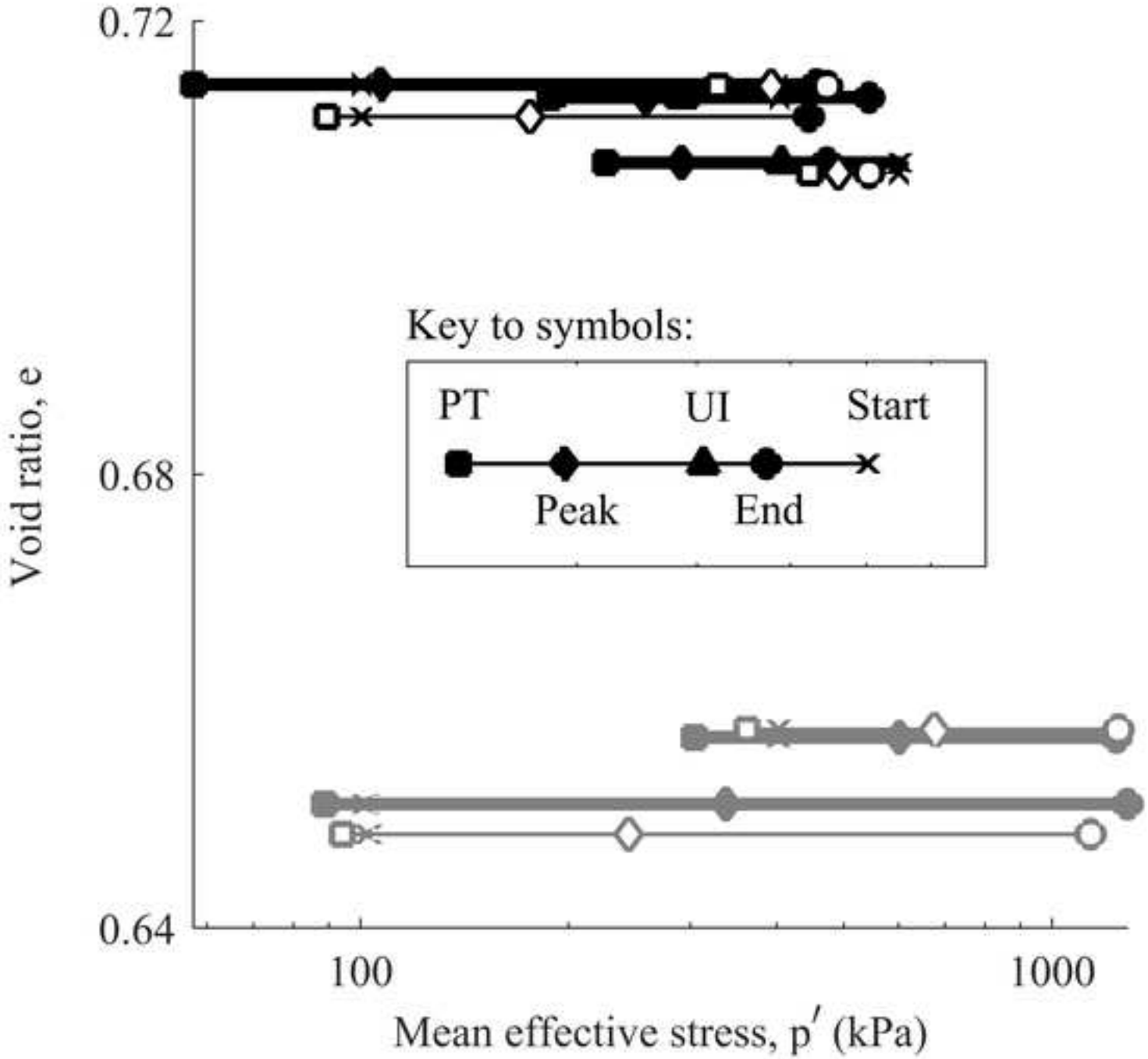

Fig 11

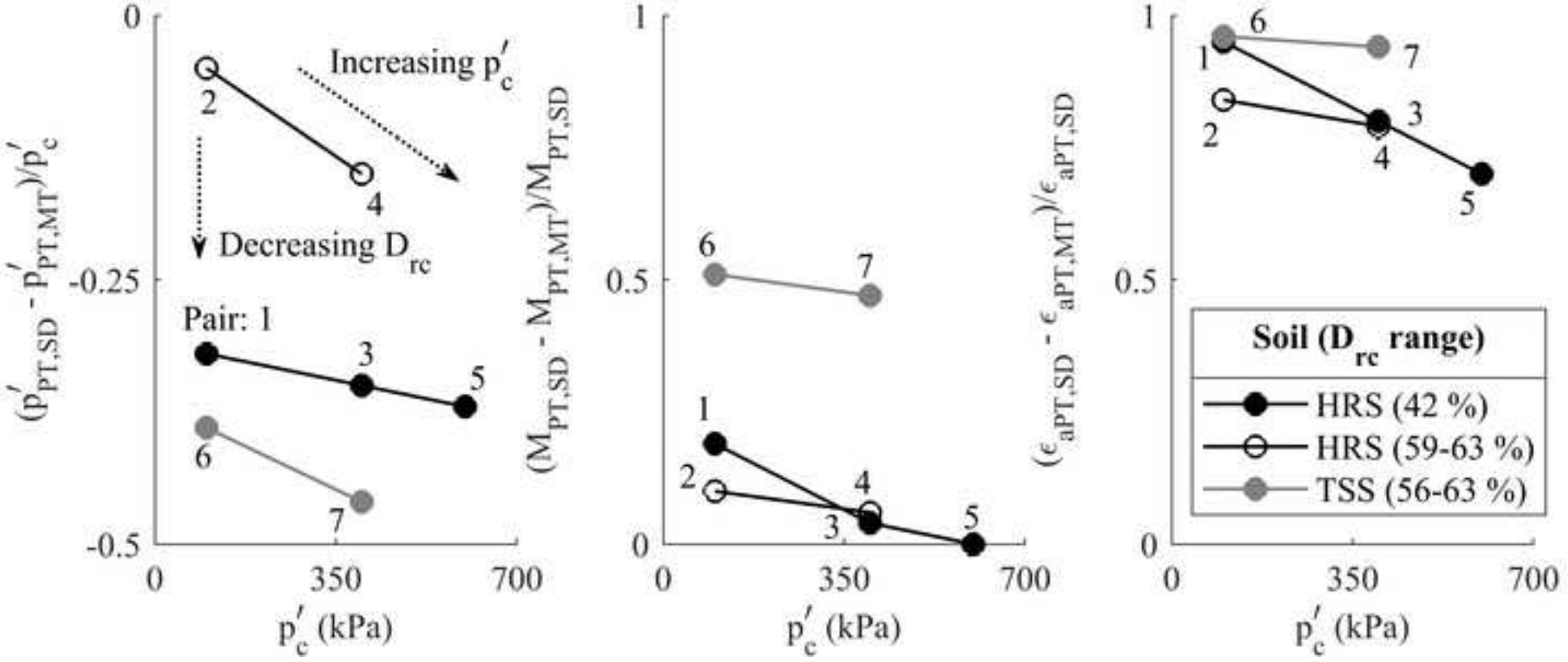

Fig 12a

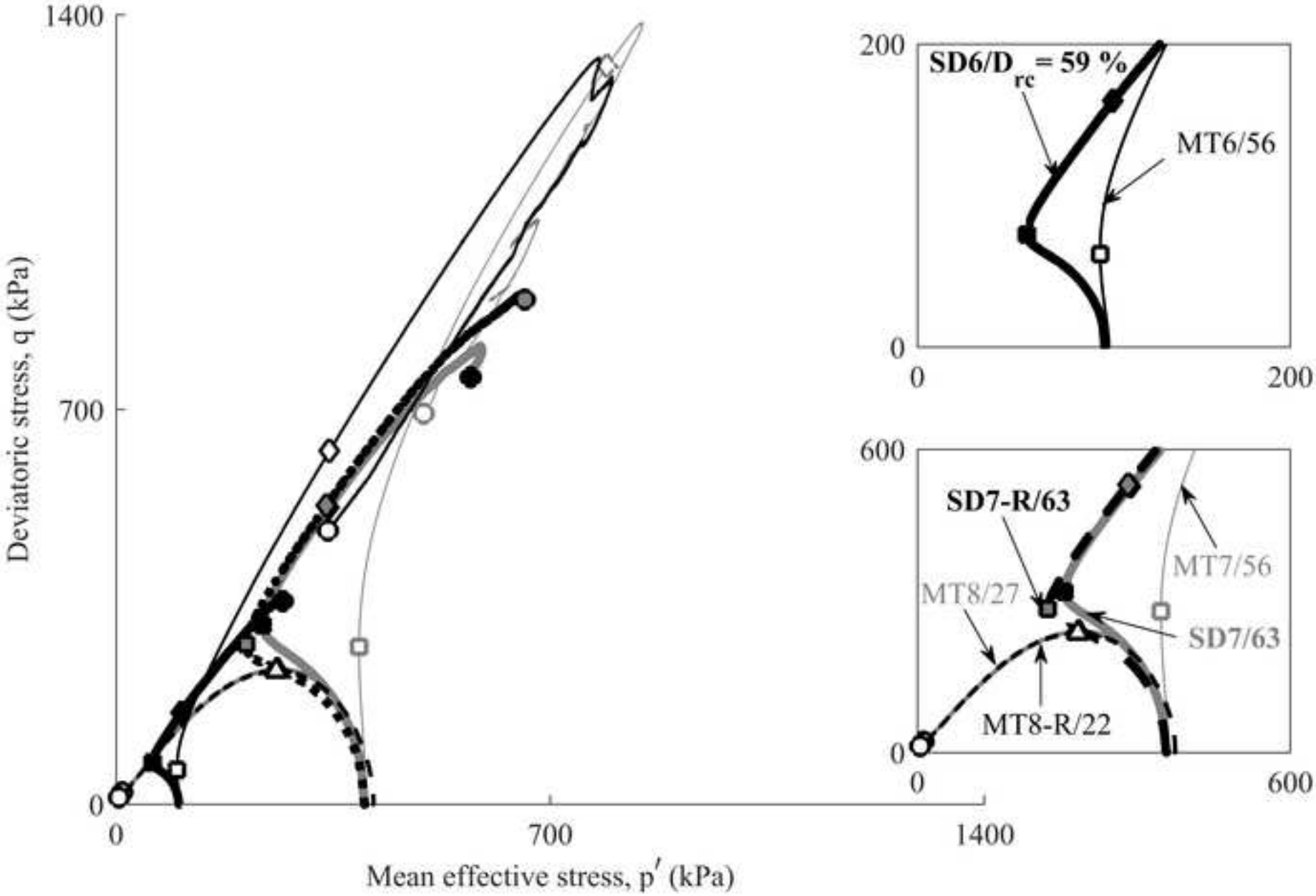

Fig 12b

Click here to access/download;Figure;Fig 12b.tif

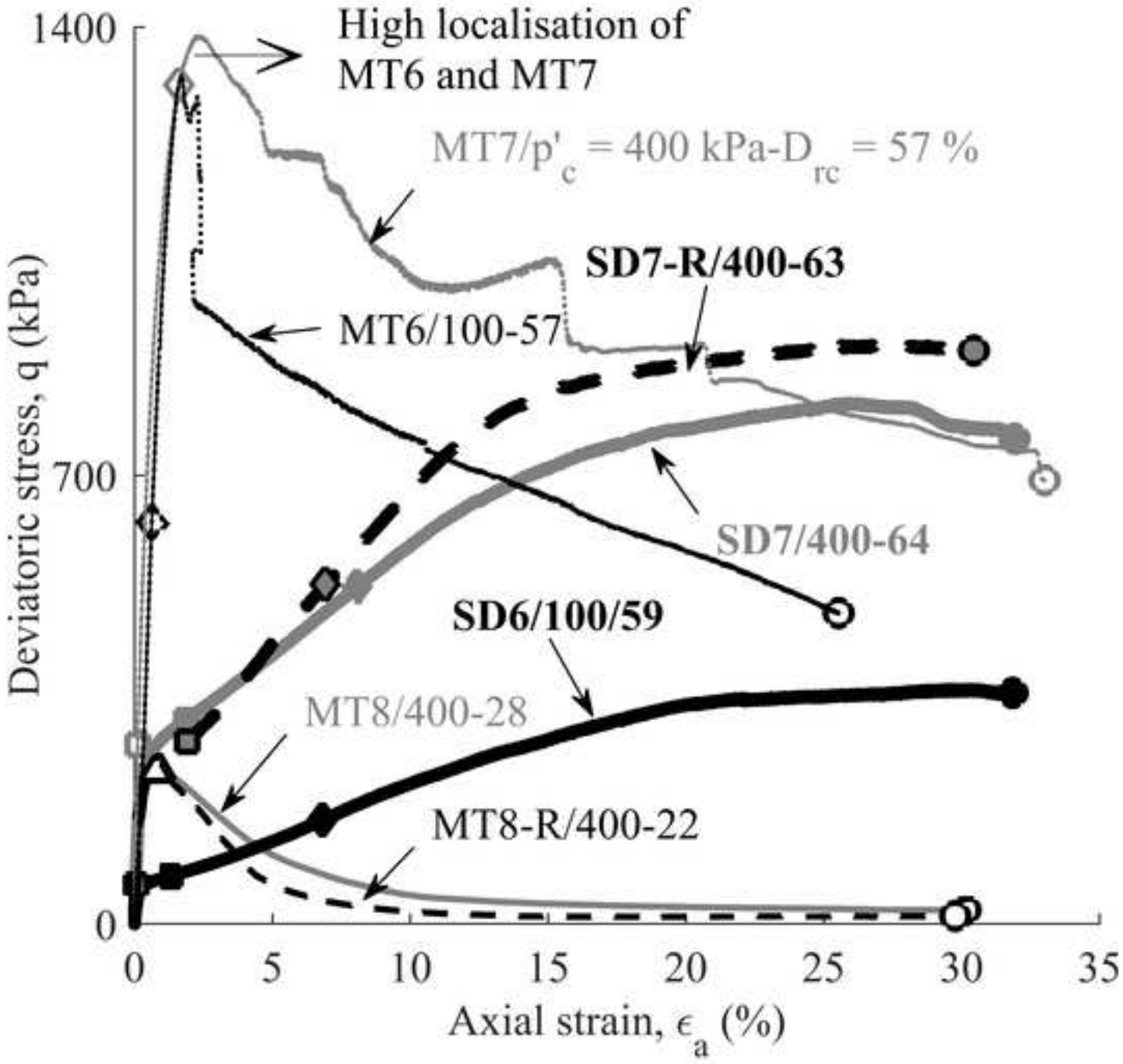

Fig 12c

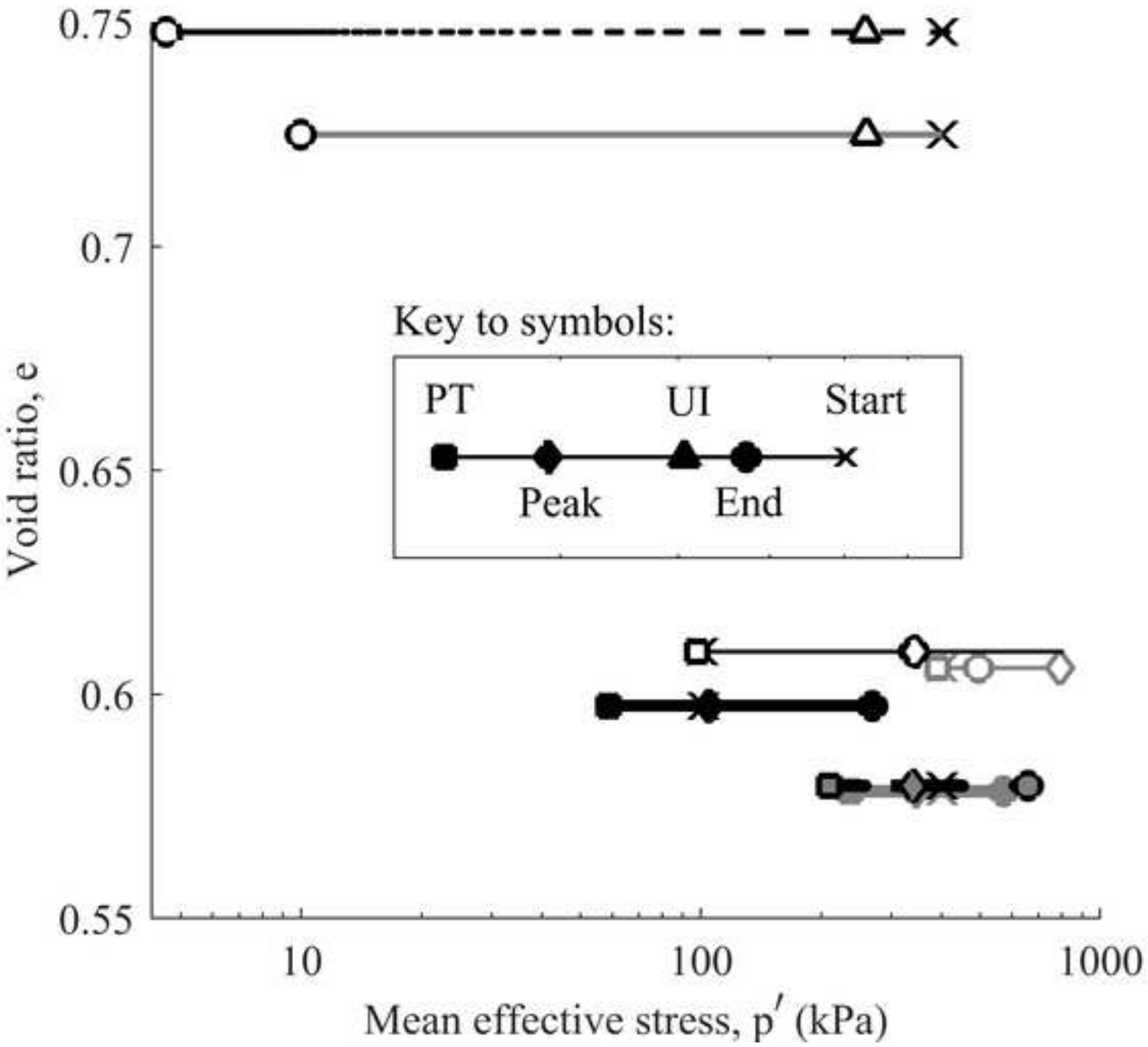

Fig 13a

Click here to access/download;Figure;Fig 13a.tif

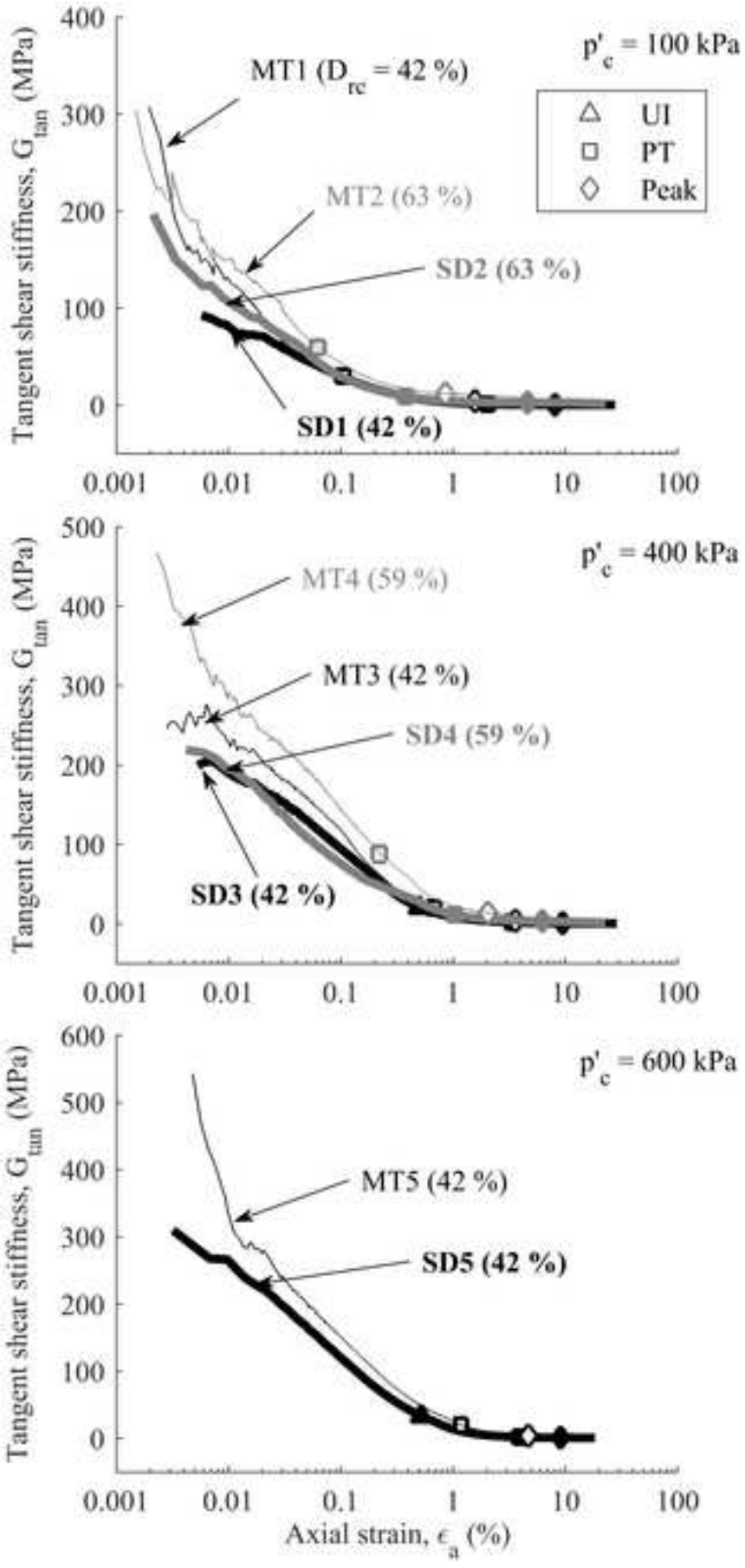

Fig 13b

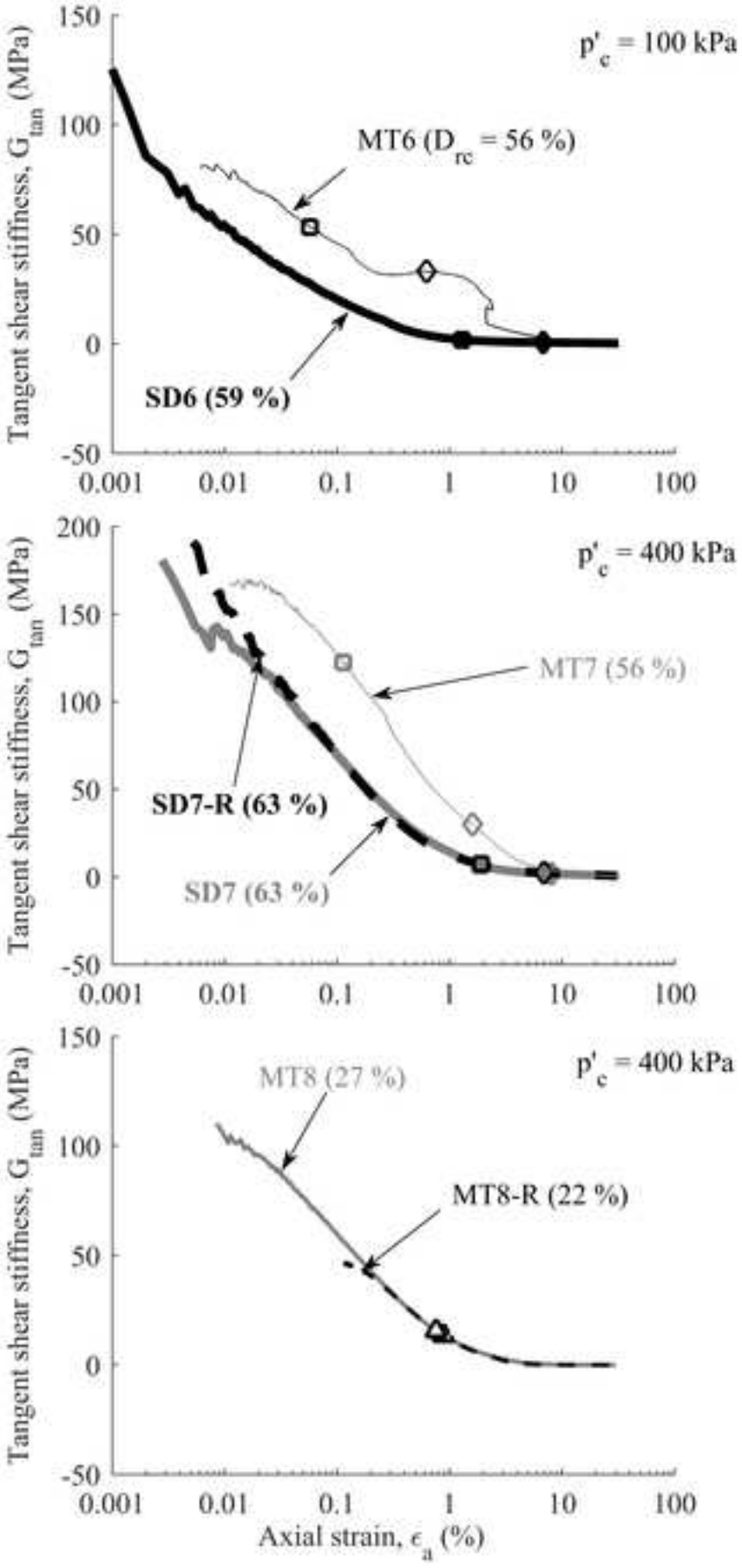

LIST OF TABLES

LIST OF FIGURES

23 Fig. 7. Slurry deposition mixing tube: schematic diagram and picture.

24 Fig. 8. Potential error due to incorrect assessment of void ratio changes during saturation for:
25 (a) loose TSS specimen MT8; and (b) various TSS specimens (effect on critical states (CS) and
26 resulting hypothetical critical state line (CSL)).

27 Fig. 9. Radial and axial strains at the end of isotropic compression.

28 Fig. 10. Undrained triaxial compression results of HRS specimens: a) stress paths, b) stress-
29 strain responses and c) compression plane responses, using SD and MT procedures as described
30 in the Specimen reconstitution section."

31 Fig. 11. Behavioral differences at phase transformation (PT) between slurry-deposited (SD)
32 and moist-tamped (MT) specimen pairs (see Table 3) as a function of consolidation mean
33 effective stress (p'_c) for: a) mean effective stress difference at PT normalised by p'_c, b) stress
34 ratio difference at PT normalised by the corresponding slurry values and c) axial strain ratio
35 difference at PT normalized by corresponding slurry values.

36 Fig. 12. Undrained triaxial compression results of TSS specimens: a) stress paths, b) stress-
37 strain responses and c) compression plane responses, using SD and MT procedures as described
38 in the Specimen reconstitution section."

39 Fig. 13. Tangent shear stiffness degradation responses of a) HRS and b) TSS specimens.

40 **TABLES**

41 Table 1. Slurry deposition studies on sandy and silty soils including uniformity analyses.

Soil type	**Uniformity analyses**				**Possible to achieve e ~ e_{max}?**	**Final deposition**	**Reference**
	PSD	Void ratio (e)	Largest variability in e	Specimen diameter			
Clean sand	Yes	Yes	0.02	63	Yes (limited by tube transfer)	Vertical; full cross-section; tube transfer	Kuerbis and Vaid (1988)
Silty sand[&]	Yes	No	N/A				
Silt	No	Yes*	0.07[+]	72	No (thick slurry)	Vertical; direct pouring	Bradshaw and Baxter (2006)
Silty sands[&]	Yes	Yes	0.01	70	Yes (limited by tube transfer)	Vertical; full cross-section; tube transfer	Carraro and Prezzi (2007)
Silt	Yes	Yes*	N/A	71	No (thick slurry)	In layers; not explained	Donahue et al. (2007)
Silt	Yes	Yes*	0.04[+]	70	No (thick slurry)	Vertical; funnel (point)	Wang et al. (2011)
Silty sand[&]	Only fines content	Yes	0.07[$]	60/100	Yes (limited by tube transfer)	Vertical; full cross-section; tube transfer	Tastan and Carraro (2013)
Silt	Yes	Yes*	0.02[+]	50	No (thick slurry)	Direct pouring; spoon mixing	Ahmadi - Naghadeh and Toker (2019)
Clean sand	Yes	Yes	0.02	38	Yes	Vertical; full cross-section	Dominguez-Quintans et al. (2019)
Silt	Yes	Yes*	N/A	36	No (thick slurry)	Vertical; direct pouring	Krage et al. (2020)
Silt	Yes	Yes	0.05	38	Yes	Vertical; full cross-section	Present study

42 *water content estimates; +assumes full saturation; [$]hollow cylinder specimens; [&]gap-graded.

43 Table 2. Index properties of materials tested.

Sample	Ham River Sand	Tailings Sandy Silt
Sample ID	HRS	TSS
Specific gravity, Gs	2.66	2.65
Uniformity coefficient, Cu	2.1	11.4
Determination coefficient, Cc	4.2	41.1
USCS group symbol	SP	ML
Particles ≤ 71 μm (%)	0	54
Maximum void ratio, ASTM[1] (dry)	0.817	1.07
Maximum void ratio, IC (under water)	0.826	0.84
Minimum void ratio	0.549[2]	0.43[3]

44 [1]ASTM D4254-16/Method B; [2]ASTM D4253-16/Method 1A; [3]ASTM D2435/D2435M − 11/slurry-deposited
45 sample, σ_v=8250 kPa.
46

47 Table 3. Changes in void ratio (e) and relative density (Drc) of specimens tested for all test stages prior to shearing.

	Specimen			Initial	After saturation			After consolidation			
Test	Pair	Soil	p_c' (kPa)	e_o	Δe	$\Delta e/e_o$	e_s	Δe	$\Delta e/e_s$	e_c	D_{rc} (%)*
SD1	1	HRS	100	0.72	0.00	0.00	0.72	0.01	0.01	0.71	42
MT1			100	0.72	0.00	0.00	0.72	0.01	0.01	0.71	42
SD2	2		100	0.66	0.00	0.00	0.66	0.01	0.02	0.65	63
MT2			100	0.65	0.00	0.00	0.65	0.00	0.00	0.65	63
SD3	3		400	0.74	0.00	0.00	0.74	0.03	0.04	0.71	42
MT3			400	0.73	0.00	0.00	0.73	0.02	0.03	0.71	42
SD4	4		400	0.67	0.00	0.01	0.67	0.01	0.01	0.66	59
MT4			400	0.67	0.00	0.00	0.67	0.01	0.01	0.66	59
SD5	5		600	0.73	0.00	0.00	0.73	0.02	0.03	0.71	42
MT5			600	0.73	0.00	0.00	0.73	0.02	0.03	0.71	42
SD6	6	TSS	100	0.61	0.00	0.00	0.61	0.01	0.02	0.60	59
MT6			100	0.61	0.00	0.00	0.61	0.00	0.00	0.61	56
SD7	-		400	0.61	0.00	0.02	0.61	0.03	0.05	0.58	63
SD7-R	7		400	0.63	0.00	0.00	0.63	0.05	0.08	0.58	63
MT7			400	0.62	0.00	0.00	0.62	0.01	0.02	0.61	56
MT8	-		400	0.81	0.02	0.02	0.79	0.06	0.08	0.73	27
MT8-R	-		400	0.81	0.01	0.01	0.80	0.05	0.06	0.75	22

48 *Drc (%) values calculated using the emax,SD value.

Table 4. Details of studies comparing intact versus reconstituted specimens or specimens from different reconstitution methods.

Materials	Reconstitution	Relative density (%)	Saturation	Void ratio assessment	Reference
Syncrude tailings sand (fine)	MT	20-50	CO_2+FL+BP	After-test specimen freezing	Sladen & Handford (1987)
Fine sands to sandy silts	AP, WS, MP	10-95	CO_2+FL+BP	N/A	Zlatovic & Ishihara (1997)
Syncrude tailings & Fraser River sands (medium, uniform)	AP, WP	~15-80	N/A	Initial specimen volume; consolidation volume changes	Vaid et al. (1999)
	MT		CO_2	After-test specimen freezing	
Natural silt + tailings sand (silty fine)	MT, SD2	~75	CO_2+BP	Initial specimen volume; no additional volume tracking; reference to post-consolidation Dr	Hoeg et al. (2000)
Wellington & Olnewville silts	SD2, MT	40-55	CO_2+BP	N/A	Bradshaw & Baxter (2006)
Gioia Tauro sand (coarse)	AP, WS	40-50	CO_2+FL+BP	N/A	Ghionna and Porcino (2006)
Clean & silty Ottawa sands	MT, SD, WP	≤65	BP	After-test water content	Murthy et al. (2007)
Clean & silty Nevada sands	DD, WS, SD, AP	30-100	CO_2+FL+BP	Cell volume changes	Wood et al. (2008)
Gold tailings silt	SD2, MT	75-100	FL+BP	N/A	Chang et al. (2011)
Toyoura sand (fine to medium)	MT, DD	20-70	CO_2+FL+BP	Specimen volume under initial saturation; reference to post-consolidation Dr	Sze & Yang (2014)
Loess silt	WC, DC, SD2	N/A	FL+BP	After-saturation specimen volume; reference to post-consolidation Dr	Xu & Coop (2017)
Mersin silt	SD2	N/A	N/A	After-saturation specimen volume	Ahmadi-Naghadeh & Toker (2019)
	MT		CO_2		
Minas Gerais tailings sandy silt	MT, SD	≤35	FL+BP	N/A	Correa & Oliveira Filho (2019)
Cuxhaven sand (fine to medium)	MT, WP, DP	60-95	N/A	Initial specimen volume; reference to post-consolidation Dr	Knudsen et al. (2019)
Tailings silt	MT, SD2	N/A	N/A	After-test specimen freezing	Reid & Fanni (2020)

MT: moist tamping; AP: air pluviation; WP: water pluviation; WS: water sedimentation; DD: dry deposition; SD: slurry deposition (self-depositing mixing tube slurry as per Kuerbis & Vaid, (1988); SD2: slurry deposition (thick slurry poured into mold); WC: wet compaction; DC: dry compaction; DP: dry pluviation; CO_2: carbon dioxide percolation; FL: water flushing; BP: back-pressure.

52 **FIGURES**